New Catalytic Systems for Light-driven Hydrogen Evolution

Li, Chuanshuai

2020

New Catalytic Systems for Light-driven Hydrogen Evolution

CHUANSHUAI LI
DIVISION OF CHEMICAL PHYSICS | FACULTY OF SCIENCE | LUND UNIVERSITY

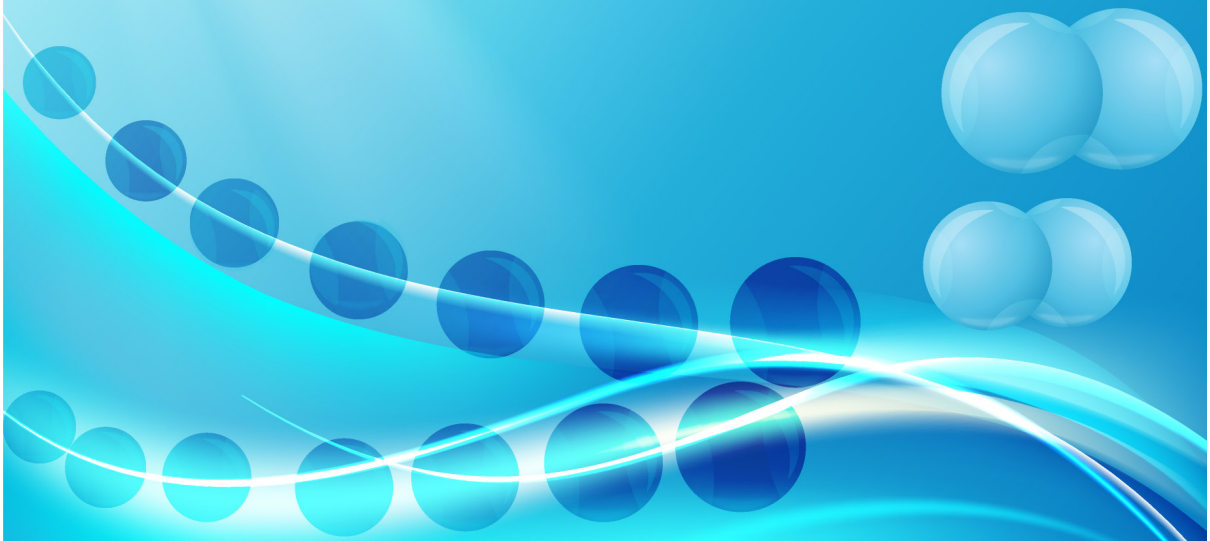

$$2H^+ + 2e^- \longrightarrow H_2$$

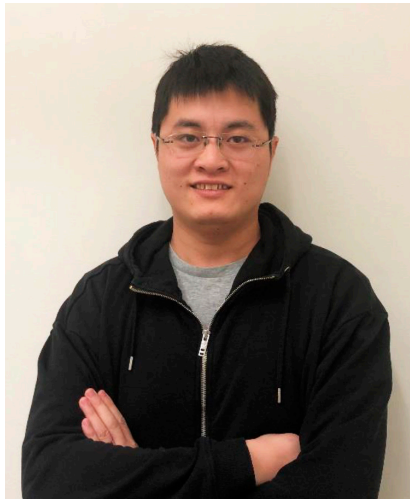

Hydrogen evolution is very simple chemical reaction, but the power it will bring to us in the future will be amazing.

Printed by Media-Tryck, Lund 2020 NORDIC SWAN ECOLABEL 3041 0903

LUND UNIVERSITY

Faculty of Science
Department of Chemistry
Division of Chemical Physics

ISBN 978-91-7422-780-2

New Catalytic Systems for Light-driven Hydrogen Evolution

New Catalytic Systems for Light-driven Hydrogen Evolution

Chuanshuai Li

LUND
UNIVERSITY

DOCTORAL DISSERTATION

by due permission of the Faculty of Science, Lund University, Sweden.
To be defended at lecture hall F, Kemicentrum, Naturvetarvägen 16, 22362 Lund.
29th of January, 2021, at 13:00

Faculty opponent
Prof. Philipp Kurz

University of Freiburg, Germany

Organization	Document name
LUND UNIVERSITY Division of Chemical Physics Department of Chemistry P.O. Box 124 SE-22100 Lund, Sweden	Doctoral Dissertation **Date of issue** 2021-01-29
Author(s) Chuanshuai Li	Sponsoring organization Chinese Scholarship Council, the Sten K Johnson Foundation

Title and subtitle
New Catalytic Systems for Light-driven Hydrogen Evolution

Abstract
Solar-driven reduction of water to produce hydrogen is one of the most promising ways to develop sustainable clean energy for the future. The challenge in photocatalytic hydrogen evolution research is to design inexpensive catalysts and construct efficient hydrogen production systems. In this thesis, different photocatalytic hydrogen production systems consisting of catalysts, photosensitizers and sacrificial agents (electron donors and proton source) has been designed and investigated based on non-precious molecular catalysts based on iron, cobalt, or molybdenum. $[Ru(bpy)_3]^{2+}$ and CdSe quantum dots were explored as photosensitizers. The photocatalytic hydrogen production of the studied systems was systematically investigated, and the attempts to establish essential steps of the mechanism of hydrogen evolution were made.

Chapter 1 gives a short introduction about photocatalytic hydrogen evolution, including semiconductor-based and $[Ru(bpy)_3]^{2+}$-based photocatalytic hydrogen evolution systems. Chapter 2 relates to papers Ⅰ and Ⅱ in the thesis, and describes the study of light-driven hydrogen evolution by CdSe quantum dot/iron carbonyl cluster assemblies and a related graphitic carbon nitride based quantum dot/iron carbonyl cluster composite. It is shown that hole transfer from CdSe quantum dots to biomimetic iron complexes dominates the fast charge transfer process and leads to enhanced hydrogen production. Chapter 3, corresponding to paper Ⅲ, describes the study of photoinduced hydrogen evolution using cobalt compounds. The primary photochemical processes of three new Co(II) complexes in the photocatalytic system have been probed by time-resolved spectroscopic analyses. Chapter 4, corresponding to paper Ⅳ, describes the study of molybdenum-organic sulfides as catalysts for photocatalytic hydrogen evolution. Time-resolved photoluminescence (TRPL) spectroscopy was used to investigate the charge carrier transfer dynamics for the photochemical properties of derivatives of $[Mo_3S_{13}]^{2-}$.

The close connection between hydrogen generating activity and charge carrier transfer dynamics in photocatalytic systems is a key theme of this thesis. Studies on the carrier dynamics can enhance the understanding of key processes in the mechanism of photocatalytic hydrogen production, and thus facilitate the design of efficient and robust photocatalytic hydrogen evolution systems.

Key words photocatalysis, hydrogen evolution, semiconductor, molecular catalyst, charge transfer, mechanism

Classification system and/or index terms (if any)

Supplementary bibliographical information		**Language** English
ISSN and key title		**ISBN** 978-91-7422-780-2 (Print) 978-91-7422-781-9 (Digital)
Recipient's notes	**Number of pages** 190	Price
	Security classification	

Signature 李传帅 Date 2020-12-15

New Catalytic Systems for Light-driven Hydrogen Evolution

Chuanshuai Li

LUND
UNIVERSITY

Coverphoto designed by Chuanshuai Li, background from Kotkoa/Freepik.

Faculty of Science
Department of Chemistry
Division of Chemical Physics

ISBN 978-91-7422-780-2 (Print)
978-91-7422-781-9 (Digital)

Printed in Sweden by Media-Tryck, Lund University
Lund 2021

Media-Tryck is a Nordic Swan Ecolabel certified provider of printed material. Read more about our environmental work at www.mediatryck.lu.se

MADE IN SWEDEN

To my family

山重水复疑无路，柳暗花明又一村。

—— 陆游《游山西村》

Table of Contents

Abstract

Solar-driven reduction of water to produce hydrogen is one of the most promising ways to develop sustainable clean energy for the future. The challenge in photocatalytic hydrogen evolution research is to design inexpensive catalysts and construct efficient hydrogen production systems. In this thesis, different photocatalytic hydrogen production systems consisting of catalysts, photosensitizers and sacrificial agents (electron donors and proton source) has been designed and investigated based on non-precious molecular catalysts based on iron, cobalt, or molybdenum. $[Ru(bpy)_3]^{2+}$ and CdSe quantum dots were explored as photosensitizers. The photocatalytic hydrogen production of the studied systems was systematically investigated, and the attempts to establish essential steps of the mechanism of hydrogen evolution were made.

Chapter 1 gives a short introduction about photocatalytic hydrogen evolution, including semiconductor-based and $[Ru(bpy)_3]^{2+}$-based photocatalytic hydrogen evolution systems. Chapter 2 relates to papers I and II in the thesis and describes the study of light-driven hydrogen evolution by CdSe quantum dot/iron carbonyl cluster assemblies and a related graphitic carbon nitride based quantum dot/iron carbonyl cluster composite. It is shown that hole transfer from CdSe quantum dots to biomimetic iron complexes dominates the fast charge transfer process and leads to enhanced hydrogen production. Chapter 3, corresponding to paper III, describes the study of photoinduced hydrogen evolution using cobalt compounds. The primary photochemical processes of three new Co(II) complexes in the photocatalytic system have been probed by time-resolved spectroscopic analyses. Chapter 4, corresponding to paper IV, describes the study of molybdenum-organic sulfides as catalysts for photocatalytic hydrogen evolution. Time−resolved photoluminescence (TRPL) spectroscopy was used to investigate the charge carrier transfer dynamics for the photochemical properties of derivatives of $[Mo_3S_{13}]^{2-}$.

The close connection between hydrogen generating activity and charge carrier transfer dynamics in photocatalytic systems is a key theme of this thesis. Studies on the carrier dynamics can enhance the understanding of key processes in the mechanism of photocatalytic hydrogen production, and thus facilitate the design of efficient and robust photocatalytic hydrogen evolution systems

Popular Science Summary

With the rapid development of industry and the massive combustion of fossil fuels, the problems of environmental pollution and energy shortage faced by mankind are becoming more and more prominent. At the same time, the massive consumption of fossil fuels will also bring about an increasingly serious energy shortage. Hydrogen is a recognized clean energy carrier and has important applications in such fields as fuels, aerospace, and rail transportation. Among the different ways to produce hydrogen, solar-driven splitting of water is one of the most promising ways to produce hydrogen on a large-scale application, which has intensively studied and made great progress in recent years.

However, the major technical bottlenecks that restrict its large-scale production have not yet made a substantive breakthrough, which requires more efforts from the scientific community. Firstly, among the reported photocatalytic systems, noble metal compounds are still mostly chosen as catalysts (e.g., precious metals such as palladium and platinum), which are expensive to produce and use, limiting the prospects for large-scale applications. Secondly, most of the catalysts reported so far suffer from low hydrogen production efficiency, poor photostability and short lifetime. In addition, in the studies of photocatalytic hydrogen evolution, more attention has been paid to the structure and composition of photocatalysts and the construction and optimization of catalytic systems, but relatively little attention has been paid to the mechanism of hydrogen production.

In this thesis, four different molecular or assembly-based proton reduction systems have been developed using noble-metal-free catalysts (iron, cobalt and molybdenum). Meanwhile, the mechanism(s) of the charge transfer processes during photocatalytic hydrogen evolution have been investigated for each system. The photocatalytic hydrogen-generating activity and stability of the different photocatalytic systems have been studied. Transient absorption and time-resolved photoluminescence spectroscopies have been used to investigate the charge carrier transfer dynamics in the catalytic systems. The close connection between photocatalytic hydrogen generating activity and charge carrier transfer dynamics is the key component in this study.

Acknowledgement

There have been so many pleasures to work and live here in Lund over the past four years. Lovely people, sweet friends, beautiful views, and easy life, all these come together into precious memories in my mind that I will enjoy forever. With the completion of my Ph.D. study, this means another adventure will soon start. However, I have to say, without the help and guidance from a number of people, it would have been impossible to finish my Ph.D. studies.

First, I would like to thank my main supervisor, Prof. Ebbe Nordlander, for giving me the opportunity to study at Lund University. He gave me a lot of freedom in my projects and taught me how to become a better chemist and researcher. I am very grateful for his guidance, support, and encouragement not only in the research. Relaxed life and efficient work are what I was always told by him and it has helped me a lot. Ebbe, thank you very much.

I would also like to thank Kaibo Zheng for his help and support in my research. I have been fortunate to be able to work and discuss with him and have gained very much knowledge from these discussions.

All my co-authors: thank you very much all for the work we did together. In particular, thanks to Yong Li, Kamal Hossain, Ahibur Rahaman, Yang Liu, Zhe Ji and Tianqiong Ma for providing the complexes and samples in my project. Thanks to Xianshao Zou, Weihua Lin, Yusen Luo, Alireza Honarfar and Mohamed Abdellah for the time-resolved spectroscopy measurements. Thanks to Meiyuan Guo for the DFT calculations. Thanks to Jie Meng, Qinying Pan and Huili Cao for XPS, BET, EDS, SEM, and TEM measurements. Thanks to Qi Shi for the power-XRD measurement. Thanks to Prof. Michael G. Richmond, Prof. Benjamin Dietzek and Prof. Omar M. Yaghi for help in my research.

I would like to thank all the present and previous members of Nordlander's group. Thanks to Hassan Mourad for helping in my research. Thanks to Lintang, Stefan, Ida, Markus, Nikolas, Fatma, Arup, Zuraan, Leandre, Brenda and Nasi. The lab cleaning and pizza time with them has been quite enjoyable. Thanks a lot for keep the lab to be a good working place with a warm atmosphere.

Thanks to all the people of Chemical Physics for making the division a great place to do research. The seminars, social activities and collaborations were so great and surprising. I want to express my thanks to Prof. Tõnu Pullerits, Prof. Arkady

Yartsev, Prof. Ivan Scheblykin, Prof. Donatas Zigmantas, Pavel Chábera and Jens Uhlig for your help and suggestions in the research, courses, and workshops. I would like to give special thanks to the KC administration staff, Anki, Maria, Caroline, Linnéa, for their help.

I would like to thank the financial support from the China Scholarship Council (CSC), the Royal Physiographic Society of Lund and the Sten K Johnson Foundation.

Thanks to so many friends I meet here, every party and outdoor activity make my life colourful. Thanks a lot for your help. Forgive me for not thanking each one of you individually - the wonderful memories stay in heart forever.

Thanks to my family for supporting me through my entire education. It hasn't been easy being away from home for most of the past 12 years. I would never have learned what I am capable of without your help.

I would like to express my greatest thanks to my wife Xiaoyan. I could not finish the Ph.D. study without all your support. Thanks a lot for your patience, tolerance, and kindness. I wish you all the best in your future. My loving son Hengche, who is the inspiration in my life - when you smiled and said baba to me, I forgot all my troubles and worries. I wish that you will grow up healthy.

Chuanshuai Li

December, 2020

Lund, Sweden

List of Publications

This thesis is based on the following papers, which will be referred to in the text by roman numbers.

I. **Chuanshuai Li**, Ahibur Rahaman, Weihua Lin, Hassan Mourad, Jie Meng, Alireza Honarfar, Mohamed Abdellah, Meiyuan Guo, Michael G. Richmond, Kaibo Zheng and Ebbe Nordlander. Electron transfer mediated by iron carbonyl clusters enhance light-driven hydrogen evolution in water by quantum dots. *ChemSusChem* **2020**, 13, 3252-3260.

II. **Chuanshuai Li**, Xianshao Zou, Weihua Lin, Hassan Mourad, Jie Meng, Yang Liu, Mohamed Abdellah, Meiyuan Guo, Kaibo Zheng, and Ebbe Nordlander, Unveiling Charge and Energy Transfer Dynamics in a g-C_3N_4/CdSe quantum dot/iron carbonyl cluster Composite that enhances Photocatalytic Hydrogen Evolution. *Submitted for publication.*

III. **Chuanshuai Li**, Yong Li, Kamal Hossain, Yusen Luo, Meiyuan Guo, Benjamin Dietzek and Ebbe Nordlander. Photoinduced hydrogen evolution catalyzed by new Co(II) complexes of N5-donor ligands. *Manuscript*

IV. **Chuanshuai Li**, Xianshao Zou, Hassan Mourad, Yong Li, Weihua Lin, Kaibo Zheng and Ebbe Nordlander. Oligomeric and Polymeric Molybdenum Sulfide Cluster Catalysts for Light-driven Hydrogen Evolution: Catalysis and Carrier Recombination Dynamics. *Manuscript*

Reprints were made with permission from the respective publishers.

Contribution to the Publications

I. I designed the experiments, synthesized the quantum dots and assemblies, performed all photocatalysis measurements and the largest part of the spectroscopic experiments, analyzed the experimental data, and drafted the manuscript.

II. I designed the experiments, synthesized the quantum dots and the composite, performed all photocatalysis measurements and the largest of the spectroscopic experiments, analyzed the experimental data, and drafted the manuscript.

III. I designed the experiments, performed all photocatalysis measurements and part of the spectroscopic experiments, analyzed the experimental data, and drafted the manuscript.

IV. I designed the experiments, performed all photocatalysis measurements and part of the spectroscopic experiments, analyzed the experimental data, and drafted the manuscript.

Abbreviations

PS	Photosensitizer
SD	Sacrificial electron donor
H_2A	Ascorbic acid
Eg	Energy gap
g-C_3N_4	Graphitic carbon nitride
MX^{++}	Methyl viologen
TEOA	Triethanolamine
EDTA	Ethylenediamine tetra-acetic acid
MPA	Mercaptopropionic acid
GSB	Ground state bleach
TON	Turnover number
TOF	Turnover frequency
DFT	Density functional theory
MeOH	Methanol
MOS	Metal-organic sulfide
DMF	Dimethylformamide
GC	Gas chromatography
NHE	Normal hydrogen electrode
CB	Conduction band
PL	Photoluminescence
QD	Quantum dot
QY	Quantum yield
TA	Transient absorption

TCSPC	Time-correlated single photon counting
TEM	Transmission electron microscopy
TRPL	Time-resolved photoluminescence
UV-Vis	Ultraviolet-visible
VB	Valence band
HER	Hydrogen evolution reaction

Chapter 1: Introduction

1.1. Green Energy : Hydrogen

A crucial scientific and technological challenge is the environmental problems associated with the extensive use of non-renewable fossil fuels. The use of renewable energy sources, such as solar, wind and tidal energy, to change the structure of energy consumption is one solution. In theory, solar energy, an almost indefinitely renewable source of clean energy, could satisfy the current and potential human energy demand. It is incredibly important that solar energy can be transformed into forms of usable energy. Nature shows us a strategy for overcoming the energy crisis by using the mechanism of photosynthesis, which uses earth-abundant water and carbon dioxide to transform solar energy to chemical fuels. There have been several attempts to achieve the direct conversion of solar energy to chemical fuels.

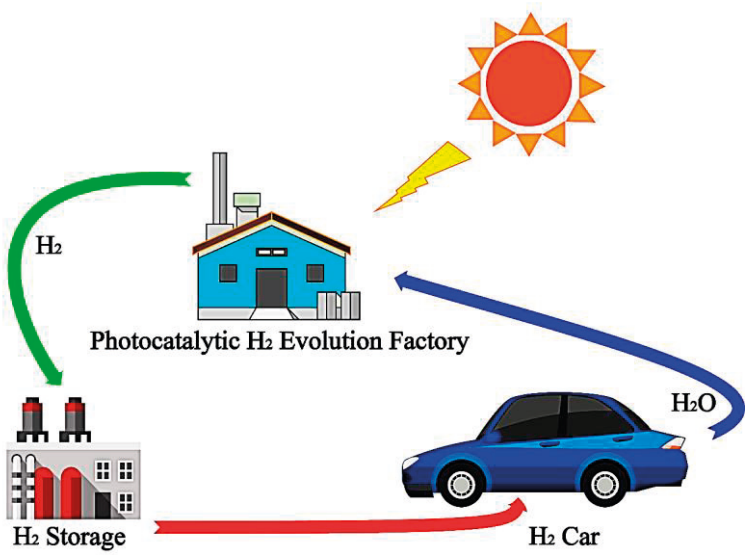

Figure 1.1. A schematic depiction of a solar-driven hydrogen energy car system.

Meanwhile, hydrogen can play a significant role in the sustainable development of a modern energy society and is used in, *inter alia*, aerospace fuels, fuel cells, industrial ammonia production and meteorological exploration. For example, there are many hydrogen-fuelled vehicles already on the market and supported by many countries (**Figure 1.1**).[1] Hydrogen can be stored, transported, and efficiently converted into electrical energy in an environmentally benign way due to its high chemical energy density of 142 MJ kg^{-1} and small molecular weight. In industry, hydrogen is produced by electrolysis of water, gasification of coal, catalytic conversion of heavy oil and natural gas vapor, etc. However, these methods of H_2 generation are energy-intensive and have low efficiencies. Therefore, researchers look for large-scale and inexpensive technologies to produce hydrogen. Hydrogen could be a solar fuel (energy carrier) that may be produced through splitting of water by artificial photosynthesis systems (**Figure 1.2**).[2,3]

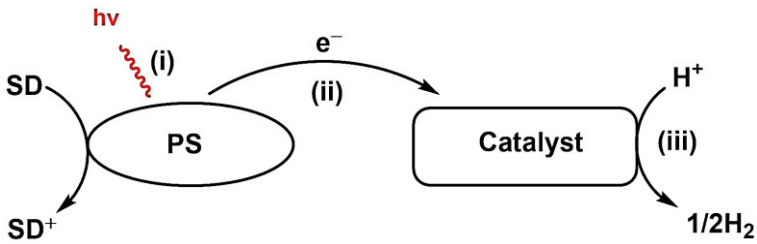

Figure 1.2. A three-component system for H_2 production (PS: photosensitizer; SD: sacrificial electron donor).

1.2. Photocatalytic Hydrogen Evolution

1.2.1. General Mechanism of Photocatalytic Water Splitting

Photocatalysis is based on the principles of photochemistry and redox catalysis. Splitting of water to hydrogen and oxygen is an endothermic reaction with a positive change in Gibbs free energy of +237 kJ mol^{-1} (Eq. (1)). It is thus an uphill reaction that requires external driving energy. Splitting of water (water reduction) can be a combination of two half reactions: proton reduction (Eq. (2)) and water oxidation (Eq. (3)).[4]

$$2H_2O \rightarrow 2H_2 + O_2 \ (\Delta G = +237 kJmol{-}1, \ \Delta E^0 = 1.23 \ V) \quad (1)$$

$$4H^+ + 4e^- \rightarrow 2H_2 \ (0V \text{ vs NHE}) \quad (2)$$

$$2H_2O \rightarrow 4H^+ + O_2 + 4e^- \ (1.23V \text{ vs NHE}) \quad (3)$$

Reduction of protons to hydrogen is a two electron-transfer process, whereas oxidation of water to oxygen is a four electron-transfer process involving sluggish kinetics. Light-induced splitting of water is possible with a photon of wavelength less than 1000 nm (equivalent to 1.23 eV), and four such photons are involved in the biological formation of one molecule of oxygen (O_2).

1.2.2. Main Process of Photocatalytic Hydrogen Evolution

Since the discovery of hydrogen evolution through the photoelectrochemical splitting of water on n-type TiO_2 electrodes,[5] (electro)photocatalytic systems for hydrogen production have been extensively studied in order to be able to apply this reaction to an industrial setting. [6-8] A photocatalytic system for light-driven H_2 evolution consists of a photosensitizer, a catalyst and sources of protons and electrons (**Figure 1.2**).[9] The reaction is first initiated by photon absorption, which generates numerous electron–hole pairs with sufficient potentials. The relevant photoreduction processes involve

(i) absorption of light by the photosensitizer and subsequent internal charge separation

(ii) intermolecular charge transfer (i.e., reduction of the catalyst by the photo-sensitizer and reduction of the photosensitizer by direct electron transfer from a sacrificial electron donor)

(iii) catalytic production of H_2 by the reduced catalyst.

The three components, photosensitizer, catalyst, and sacrificial agent, play important roles in these three processes. Finding a suitable three-component system for photocatalytic hydrogen production and performing mechanistic studies on such systems remain great challenges.

The photosensitizer in the photocatalytic reduction of protons functions as light absorber and a supplier of electron(s) to the catalyst. Ideal photosensitizers should have large extinction coefficients over a broad spectral range, long excited state lifetimes, and excellent photostability. Various photosensitizers involving chromophores such as organic molecules, coordination complexes (e.g. $[Ru(bpy)_3]^{2+}$) and organometallic complexes, as well as quantum-confined semiconductor nanocrystals (quantum dots) have been developed.[10-12] Organometallic chromophores are mostly used in homogeneous photocatalytic hydrogen evolution. Their stabilities and long lifetime properties make them good candidates to use as photosensitizers when the catalytic performances of different molecular catalysts are studied and compared. Semiconductors, including semiconductor quantum dots, have many characteristics that are ideal for light-harvesting and electron delivery. Compared with organic and organometallic chromophores, semiconductor quantum dots offer unique size-dependent

absorption properties, large absorption cross sections over a broad spectral range, long excitation lifetimes, and superior photostability.[13] Quantum dots can simultaneously absorb multiple photons, or continuously absorb multiple photons even after electrons or holes are accumulated, thus enabling the coupling of single-photon/electron events with multiple-electron redox reactions necessary for photocatalytic H_2 production. The surfaces of quantum dots can be readily modified for specific functional targets and/or reaction environments and can thus be used to form molecular assemblies with the catalysts and/or sacrificial electron donors. These characteristics make quantum dots superb candidates as photosensitizers for photocatalytic generation of hydrogen.

Efficient and long-lasting functional catalysts for light-harvesting, charge transport, and redox reactions are required by a technologically significant solar-driven H_2 production system. While metallic colloidal platinum or molecular platinum complexes show excellent activities for H_2 production, platinum is scarce and expensive.[7] Catalysts relying on noble-metal free materials are therefore desirable.[8,14] The natural hydrogenase enzymes (H_2ases) have active sites consisting of organometallic entities containing the earth-abundant elements iron and, in some cases, nickel, which exhibit remarkable capacities for reduction of protons to H_2 (6000–9000 molecules of H_2 per second per active site).[15] The special working environments and oxygen sensitivities of these enzymes lead to limitations in large-scale application of natural hydrogenases for hydrogen production. Because of the structural relation to active sites of certain hydrogenases, biomimetic diiron complexes have been investigated in catalytic systems for hydrogen evolution.[16] Despite many attempts to develop efficient photocatalytic systems based on such biomimetic complexes, the development of efficient base metal (e. g. iron and cobalt) catalysts for hydrogen evolution systems remains a significant challenge.[17]

The sacrificial electron donor provides electrons for the reductive half-reaction of the artificial photosynthesis, in the absence of photogenerated electrons.[2] Commonly used sacrificial electron donors include tertiary amines, alcohols, and ascorbic acid.[5] Generally, such sacrificial electron donors undergo decomposition following one electron oxidation, and such degradation produces proton(s). Thus, many sacrificial electron donors can function not only as the source of electrons but also the source of protons.

Several photocatalyst systems that can drive water splitting under light irradiation have been identified, and mechanisms, roles of different components, as well as physical and optical properties of the photocatalysts for water splitting have been

elucidated.[8,9,13] However, it is still a formidable challenge to improve the efficiency of photocatalytic systems and to find stable solar-to-hydrogen transformation pathways.

1.3. Semiconductor-based Photocatalytic Hydrogen Evolution Systems

1.3.1. Fundamental Mechanism of Semiconductor-based Photocatalytic Hydrogen Evolution

The fundamental mechanism of semiconductor-based photocatalysis is relatively well understood, and it is illustrated in **Figure 1.3**. Such heterogeneous photocatalysis involves seven key steps, which may be classified into four major processes: light absorption (step 1); charge excitation (step 2); charge separation, transfer, and recombination (steps 3, 4 and 5) and surface catalytic reactions (steps 6 and 7). Generally, an electron in the valence band (VB) of the semiconductor could be excited to its conduction band (CB) under irradiation of light with energy higher than or equal to the band gap energy (Eg) of the semiconductor, leaving a positive hole in the VB. This stage is referred to as the "photo-excited" state of the semiconductor, and the band gap energy corresponds to the wavelength of the light that is effectively absorbed by the semiconductor. After photoexcitation, the excited electrons and the holes migrate to the surface of the semiconductor to facilitate both the reduction and oxidation of H_2O. Charge recombination, including both surface and bulk recombination of electrons and holes, reduces the excited charges by emitting light or generating phonons; this is a deactivation process and ineffective for hydrogen production. There are two keys to developing a suitable semiconductor with high efficiency for light-driven hydrogen evolution: (1) the semiconductor should possess a suitable band gap and structure (2) charge separation in the semiconductor should be efficient.[18] A wide range of semiconducting materials have been developed as catalysts for photocatalytic hydrogen evolution (e.g. colloidal quantum dots and graphitic carbon nitride).[9,13,19]

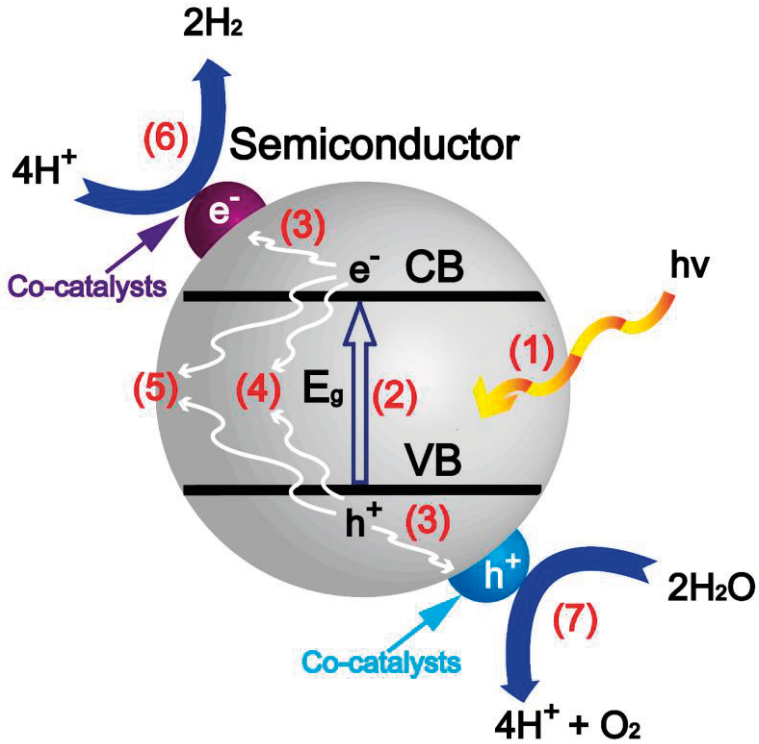

Figure 1.3. The fundamental mechanism of semiconductor-based photocatalysis. The typical steps are: (1) light absorption; (2) and (3) charge excitation, separation and transfer; (4) charge recombination in bulk; (5) charge recombination on surface; (6) surface reduction reactions; and (7) surface oxidation reactions.

1.3.2. Semiconducting Quantum Dots for Photocatalytic Hydrogen Evolution

Semiconductor nanocrystals (also known as quantum dots, QDs) can greatly improve and enhance the stability and hydrogen production performance of photocatalytic systems when used as photosensitizers.[20] Quantum dots are nanoparticles that are mainly composed of II-VI and III-V elements and their sizes typically fall in the range of 1-10 nm. Approximately 40 % of sunlight is visible light, and an ideal absorber would harvest as much visible light ($\lambda < 800$ nm) as possible to afford high populations of charge carriers that are sufficiently energetic for the redox reactions involved in artificial photosynthesis. With an understanding of quantum confinement,[21] one can readily tune the bandgap of QDs to cover a very broad range of the solar spectrum. For example, materials can be generated that absorb nearly all visible light by controlling the size distributions of cadmium selenide quantum dots (**Figure 1.4**). The methods of preparation of quantum dots are divided into two kinds: syntheses using an organic solvent at high temperatures (>300°C) and syntheses in aqueous solution at low temperatures (<100°C). In this

thesis, the focus is on preparation of quantum dots in aqueous solution. By introduction of appropriate protective groups or ligands, water-soluble quantum dot nanoparticles can be prepared.[22-24]

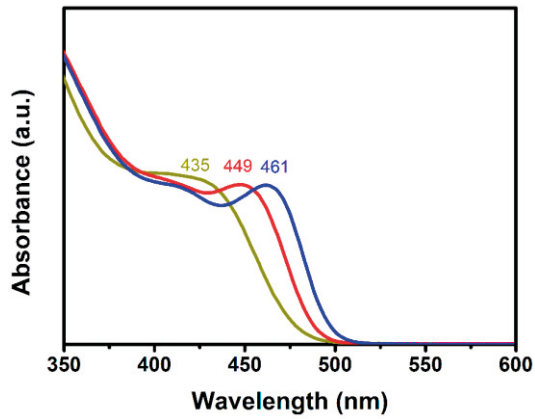

Figure.1.4. UV-Vis spectra of different sizes of CdSe quantum dots: D_{p435}=~1.9 nm, D_{p449}=~1.95 nm and D_{p461}=~2.0 nm.[25]

1.3.3. Graphitic Carbon Nitride (g-C_3N_4) Photocatalytic Hydrogen Evolution

Graphitic carbon nitride (g-C_3N_4) based photocatalysts have attracted increasing interest since Wang and coworkers first discovered photocatalytic H_2 and O_2 evolution over C_3N_4 in 2009.[26] Graphitic carbon nitride has a layer-like stacking structure similar to that of graphitic carbon with sp^2 hybridized carbons and nitrogens, with a conjugated electron energy band structure (**Figure 1.5**). Graphitic carbon nitride thus has a visible light response of 2.7 eV, and the corresponding absorption edge (460 nm) is in the visible region (400-700 nm). Through the traditional thermal condensation of several low-cost N-rich organic solid precursors such as urea, thiourea, melamine, dicyandiamide, cyanamide, and guanidine hydrochloride, g-C_3N_4 can be readily produced in air or inert atmosphere at 500-600 ^oC.[27] Rich surface properties, non-toxicity, abundance, and good stability of g-C_3N_4 give access to a wide variety of applications of the material in sustainable chemistry as a multifunctional heterogeneous metal-free photocatalyst.[28] However, the fast recombination of photogenerated charge carriers leads to low efficiency of hydrogen evolution in pure g-C_3N_4 systems. Therefore, various strategies are employed to suppress the recombination of charge carriers in g-C_3N_4 in order to promote the photocatalytic performance; examples of such strategies include textural design, supramolecular-chemistry methods, elemental doping and copolymerization, and the construction of g-C_3N_4-based heterojunction nanohybrids.[28]

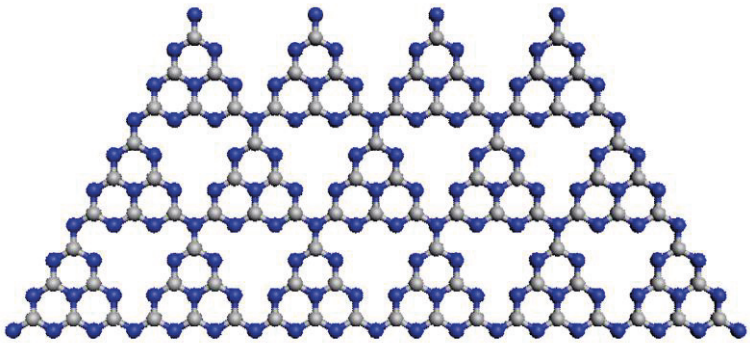

Figure 1.5. A structure diagram of graphitic carbon nitride (g-C_3N_4). The grey balls:C; blue balls: N.

1.4. $[Ru(bpy)_3]^{2+}$-based Photocatalytic Hydrogen Evolution Systems

The complex $[Ru(bpy)_3]^{2+}$ and its related complexes are classical photosensitizers with high stabilities, long lifetime properties, and are mostly used in homogeneous photocatalytic hydrogen evolution.[10,11] Typically, a $[Ru(bpy)_3]^{2+}$ based photocatalytic hydrogen evolution process is initiated by light absorption of the photosensitizer, generating an excited state that can be quenched by electron transfer through a reductive or an oxidative reaction pathway (**Figure. 1.6**).[29] The reductive quenching of the photoexcited state $*[Ru(bpy)_3]^{2+}$ involves an electron transfer from a sacrificial electron donor to generate the reduced form $[Ru(bpy)_3]^{+}$, which can transfer an electron to the catalyst and return to its ground state $[Ru(bpy)_3]^{2+}$. The second reaction pathway for H_2 production is based on an oxidative quenching of $*[Ru(bpy)_3]^{2+}$ by the catalyst affording the oxidized form $[Ru(bpy)_3]^{3+}$, which returns to its initial form $[Ru(bpy)_3]^{2+}$ after an electron transfer from the sacrificial electron donor.

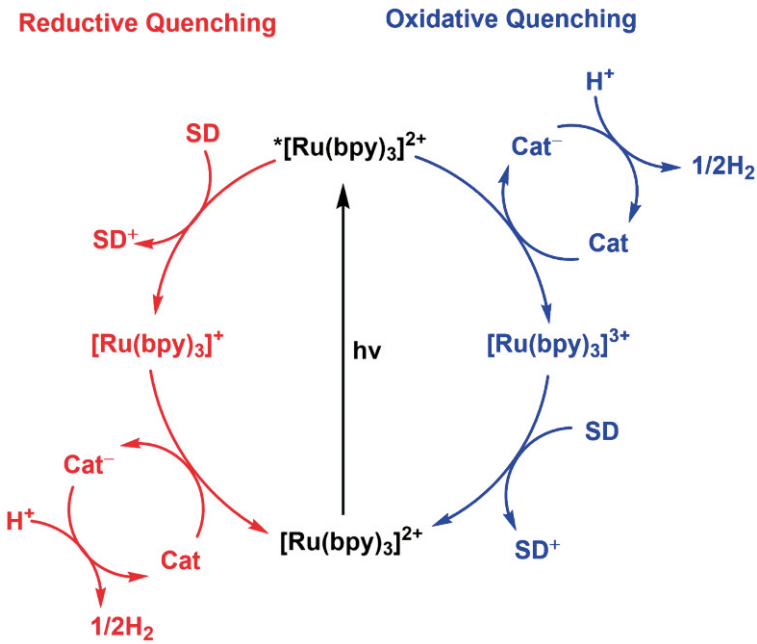

Figure. 1.6. General mechanisms of H_2 production from a photocatalytic system containing a photosensitizer $[Ru(bpy)_3]^{2+}$, a catalyst (Cat) and a sacrificial electron donor (SD).

Proof of principle for artificial photosynthesis with molecular species was first reported in 1977 by Lehn and coworkers who showed that hydrogen could be produced by irradiation using the combination of $[Ru(bpy)_3]^{2+}$ as photosensitizer, $[Rh(bpy)_2Cl_2]^{+}$ as electron mediator, triethanolamine (TEOA) as sacrificial electron donor, and K_2PtCl_6 as a precursor to Pt colloids that serve as the catalysts for proton reduction.[30] Similar systems developed by Grätzel and Kagan closely followed that of Lehn and coworkers, using $[Ru(bpy)_3]^{2+}$ as photosensitizer, methyl viologen (MX^{++}) as electron mediator, and TEOA and ethylenediamine tetra-acetic acid (EDTA) as electron donors, respectively.[31,32] Most notably, these latter studies investigated the mechanism of hydrogen formation more thoroughly through flash laser photolysis and identified oxidative quenching of the ruthenium photosensitizer as the pathway for electron transfer.

Chapter 2: Semiconductor/Molecule-based Systems for Light-driven H_2 Evolution (Papers I and II)

Solar-driven water reduction is one of the most important promising strategies for production of hydrogen to meet the huge energy demand in modern society. As discussed in Chapter I, a typical photocatalytic hydrogen evolution system consists of a catalyst, a photosensitizer, and a sacrificial electron donor. Semiconductors show excellent light absorption abilities and can thus be used as photosensitizers to construct highly efficient and durable photocatalytic systems.[33] The catalysts in the reductive half reaction of water reduction receive electrons from the photophysically excited state (the valence band) of the semiconductor. Numerous catalysts have been explored as replacements for the precious platinum complexes or colloidal platinum particles that are the best-known catalysts for the hydrogen evolution reaction.[34] There are several ways to combine semiconductor photosensitizers (e.g. quantum dots) with base metal proton reduction catalysts to form photocatalytic systems.[35]

2.1. Quantum Dot/Molecule Systems for Photocatalytic Hydrogen Evolution

Hydrogenase enzymes are natural catalysts for hydrogen production with remarkable turnover frequencies.[36] After the discovery of the active site structure of [FeFe]-hydrogenases, intense research on biomimetic iron complexes has been carried out in order to develop chemical and photochemical catalyst systems for H_2 production.[37] The construction of assemblies consisting of quantum dots and molecular iron complexes provides an efficient way to prepare water soluble catalysts with enhanced activity for the photocatalytic hydrogen evolution reaction. The first example of the association of a water soluble bioinspired diiron catalyst, **2.1** (Figure 2.1), with 3-mercaptopropionic acid (MPA)-stabilized CdTe quantum dots, and the use of the resultant assembly for photocatalytic H_2 production, was reported in 2011 by Wu and co-workers.[38] The molecular assembly was able to

achieve H_2 production with a TON of up to 505, with ascorbic acid acting as the proton source and electron donor. The researchers suggested that the interaction between the quantum dot and **2.1** dominates the enhancement of hydrogen evolution compared with the HER activity of pure CdTe quantum dots. Similar assemblies based on a series of [FeFe]-H_2ase mimics (**2.2**, **2.3** and **2.4**) and quantum dots have been developed for light-driven hydrogen evolution (**Figure 2.1**).[39-41] In paper I, a new assembly consisting of CdSe quantum dots that are coupled with a triiron molecular complex/catalyst,[42,43] *viz*. $[Fe_3Te_2(CO)_9]$ (**2.5**), prepared using an interface-directed approach, has been tested as a catalytic system for hydrogen production in a water/acetonitrile solution.[25]

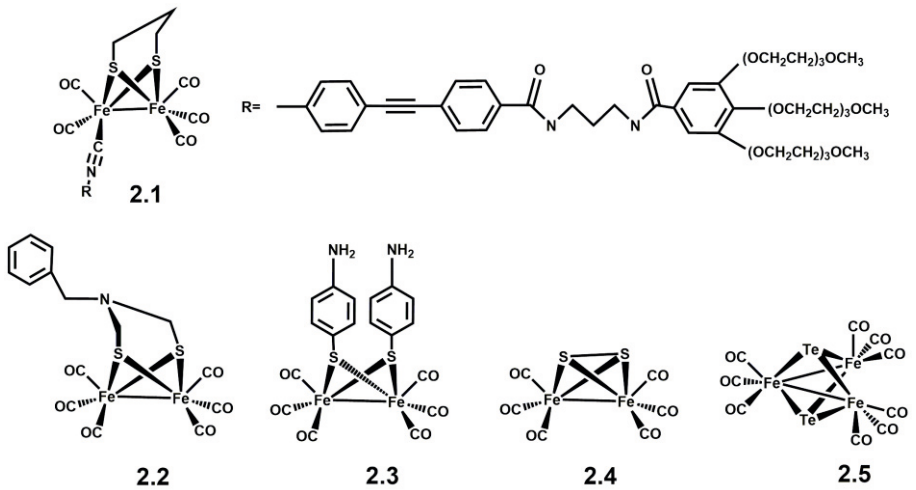

Figure 2.1. Structures of [FeFe]-H_2ase mimics **2.1**–**2.4** used as catalysts in hybrid systems with CdSe, CdTe or ZnS quantum dots as light harvesters. Structure of the triiron carbonyl cluster **2.5** used in the present work.

Besides assemblies of quantum dots with iron complexes, some other effective photocatalytic systems for hydrogen production based on quantum dots and metal complexes or metal salts have been reported.[44-46] Photocatalytic systems containing $Ni(NO_3)_2$, $NiCl_2$, or $Ni(acetate)_2$ with dihydrolipoic acid (DHLA)-capped CdSe quantum dots produce hydrogen with turnover numbers >600,000 after 360 h of illumination with visible light at pH 4.5.[44] Other systems where CdSe quantum dots capped by a tripodal thiolate are used as sensitizers and one of five square planar Ni(II) bis(chelate) complexes as catalyst gave hydrogen evolution turnover numbers in excess of 100,000.[45] Three cobaloxime catalysts (**2.6**–**2.8**) were proposed to be weakly adsorbing on CdS nanosheets to construct efficient photocatalytic systems showing good proton reduction activities (**Figure 2.2**).[46] Huang et al. selected CdSe/ZnS core/shell quantum dots as photosensitizers and another cobaloxime molecular catalyst (**2.9**) to fabricate photocatalytic systems,[47] and other photocatalytic systems constructed with CdTe quantum dots as photosensitizers, cobalt(III) complexes (**2.10**–**2.11**) as molecular catalysts and

ascorbic acid as sacrificial electron donor were reported by Llobet and co-workers.[48] The advantages of both semiconductors and molecular catalysts can be combined in these types of assemblies.

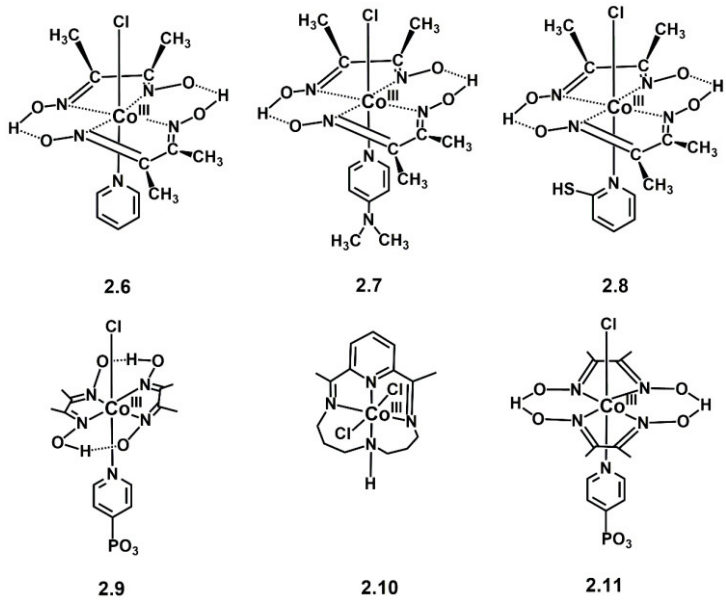

Figure 2.2. Structures of Co complexes **2.6**–**2.11** used as catalysts in hybrid systems with quantum dots as light harvesters.

2.2. Charge Transfer Dynamics in Semiconductor/Molecule Systems for Photocatalytic Hydrogen Evolution

Although various semiconductor/molecule systems or assemblies have been reported, the kinetic mechanisms, especially charge transfer between semiconductors and molecular catalysts, need to be investigated.[49] Charge transfer is a key step for achieving high efficiency of hydrogen production in a photocatalytic system. Charge transfer can occur when the (electronic) energy levels of the donor and acceptor match the thermodynamic requirement to overcome the interface boundary between the semiconductor and the molecular catalyst. The charge transfer dynamics can be affected by the semiconductor's intrinsic structure, surface properties, size and morphology, and also the redox potential of the molecular catalysts in proton reduction.[50] For example, 3-mercaptopropionic acid (MPA) is often used as a capping ligand for quantum dots. The presence of MPA ensures charge balance and stability of the quantum dots in

solution.[22-24] However, fast hole trapping occurs in excited MPA-capped quantum dots.[51] Such trapping of charge carriers in the surface state of quantum dots is a common occurrence and plays an important role in photocatalytic hydrogen evolution processes.

Slowing down the recombination in the semiconductor itself and accelerating the interfacial charge transfer is considered to be the main methodology to ensure efficient photocatalytic hydrogen production. Studies on interfacial charge transfer are mainly focused on charge transfer rates and charge separation efficiency. In a study on hydrogen evolution by and charge transfer dynamics in a CdSe quantum dot/[$Fe_2S_2(CO)_6$] assembly, a transient absorption decay rate for the assembly was found to be 8.8 ns shorter than that of the CdSe quantum dots alone (17.6 ns), and this was interpreted to indicate the occurrence of electron transfer from the CdSe quantum dots to the iron cluster with concomitant efficient H_2 evolution.[40] Interfacial electron transfer with a picosecond time constant was observed by Huang et al. in photocatalytic systems based on CdSe/ZnS core/shell quantum dot photosensitizers and cobaloxime complex **2.9** as HER catalyst.[47] Hybrid systems containing water-soluble CdTe quantum dots and a molecular catalyst - either a macrocyclic cobalt(III) complex (**2.10**) or a phosphonate-functionalized cobalt(III) bisglyoximate complex (**2.11**) - have been investigated by Palomares, Llobet, and co-workers to explore the kinetics of charge transfer.[48] In these hybrid systems, the direct electron transfer from the excited CdTe quantum dots to the cobalt catalysts and interfacial hole transfer from the CdTe quantum dots to ascorbic acid both occur on the nanosecond timescale while the back electron transfer occurs on the millisecond timescale. The catalytic reaction proceeds much slower with a rate on the microsecond scale. The charge transfer dynamics differ in different semiconductor/molecular systems, but it provides important information to understand the key reaction steps in the photocatalytic hydrogen production process.

2.3. Graphitic Carbon Nitride-based Composites for Photocatalytic Hydrogen Evolution

In addition to traditional semiconductor quantum dots, multidimensional semiconductors, such as polymeric graphitic carbon nitride (g-C_3N_4), have been considered to be good and robust candidates for photocatalytic hydrogen evolution, in combination with molecular catalysts or semiconductors (e.g. quantum dots).[52,53] In such systems, the photocatalytic efficiency of the semiconductor materials have been improved by incorporation of semiconductor heterojunctions, in which the photogenerated electron−hole pairs can be efficiently separated and transferred to the active sites for (separate) reactions in a catalytic system.[54,55]

With regard to the band gap and the potentials of the valence band (VB) and conduction band (CB) of semiconductors, the electronic structure of the coupled composites can be categorized into several classifications, i.e. Type I (straddling gap), Type II (staggered gap), Type III (broken gap), Z-scheme heterojunctions and Schottky junction (**Figure 2.3**).[52] In the Type I heterojunction (**Figure 2.3** (a)), the VB and CB of semiconductor 1 are lower and higher than those of semiconductor 2, respectively. When semiconductor 1 is excited under light irradiation, photogenerated holes can be transferred from the VB of semiconductor 1 to the VB of semiconductor 2, while the electrons can transfer from the CB of semiconductor 1 to the CB of semiconductor 2. Type II heterojunctions (**Figure 2.3** (b)) can significantly promote the separation of electrons and holes to retard their recombination and thus achieve an efficient composite for photocatalytic hydrogen evolution. The photogenerated holes in the VB of semiconductor 2 can transfer to that of semiconductor 1, while the photogenerated electrons in the CB of semiconductor 1 can migrate to that of semiconductor 2, resulting in a spatial separation of charge carriers. In Type III heterojunctions (**Figure 2.3** (c)), there is no photogenerated charge transfer between two semiconductors. Z-scheme heterojunctions (**Figure 2.3** (d) and (e)) have been reported to efficient charge transfer systems during the photocatalytic process.[56] The Schottky junction (**Figure 2.3** (f)) consists of a semiconductor and metal-like material, which is

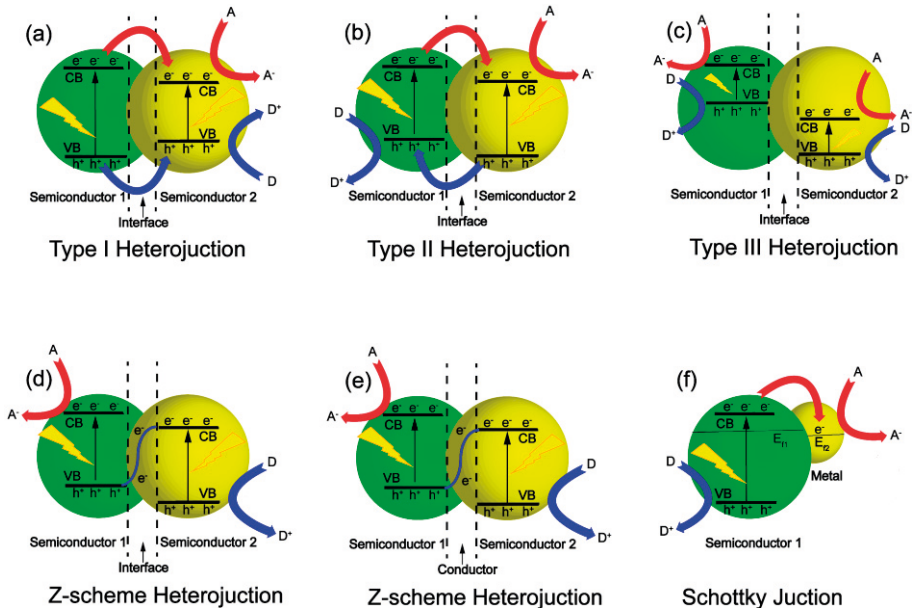

Figure 2.3. Schematic energy band diagram of three different types of heterojunctions in a typical semiconductor hybrid nanocomposite adapted from (52): (a) Type I heterojunction, (b) Type II heterojunction, and (c) Type III heterojunction, (d) Semiconductor−semiconductor Z-scheme heterojunction, (e) semiconductor−conductor−semiconductor Z-scheme heterojunction, (f) Schottky junction of metal/semicomductor nanohybrids. A and D denote electron acceptor and electron donor, respectively.

beneficial in constructing a space-charge separation region. Understanding which type of heterojunction that is formed is important in the design of g-C_3N_4 based composites with other semiconductors (quantum dots) and to enable improvement of the efficiency of charge separation during photocatalytic hydrogen evolution.

Type II SnO_2−ZnO/g−C_3N_4 heterostructure hybrids have been prepared by Byon and coworkers; in these hybrids, SnO_2−ZnO quantum dots are anchored to g−C_3N_4 nanosheets via an in situ co−pyrolysis approach.[57] The resultant hybrids exhibited excellent photocatalytic performance for hydrogen evolution under visible−light irradiation with outstanding cycling stability. In another type II Au/TiO_2–g−C_3N_4 nanocomposite hybrid system constructed by Clément et al., a remarkably efficient photocatalytic hydrogen production resulted from simultaneous favourable nanoheterojunction formation between g−C_3N_4 and TiO_2 semiconductors, as well as Au nanoparticle/g−C_3N_4 and Au nanoparticle/TiO_2 junctions.[58] Zhong et al. created type II CdSe quantum dot/g−C_3N_4 composites that were found to significantly enhance photocatalytic hydrogen production compared with pure CdSe and g−C_3N_4. This positive effect was attributed to the synergism of excellent visible absorption and high charge separation efficiency from the heterostructures.[55] Besides the above studies, there are few reports on research about the incorporation of quantum dots into g−C_3N_4.

2.4. CdSe Quantum Dots/Iron Carbonyl Cluster Assemblies as Photocatalytic Hydrogen Evolution Systems

In paper I, assemblies of CdSe quantum dots with iron chalcogenide carbonyl clusters are described. The previously known CdSe quantum dot/[$Fe_2S_2(CO)_6$] assembly and the new CdSe quantum dot/[$Fe_3Te_2(CO)_9$] assembly were tested as catalytic systems for hydrogen production in aqueous solution or aqueous/organic mixture solution. The structure, chemical composition, and optical properties of the prepared samples were investigated via a series of characterization techniques. In the presence of ascorbic acid as a sacrificial electron donor and proton source, these assemblies were found to exhibit enhanced activities for the rate of hydrogen production under visible light irradiation, with considerably better performance than that of pure CdSe quantum dots under the same conditions. The CdSe quantum dot/[$Fe_3Te_2(CO)_9$] assembly shows a better hydrogen production result than the CdSe quantum dot/[$Fe_2S_2(CO)_6$] assembly under the same experimental conditions. Transient absorption and time-resolved photoluminescence

spectroscopies were used to investigate the charge carrier transfer dynamics in the quantum dot/iron carbonyl cluster assemblies.

In CdSe quantum dot systems, the ground state bleach (GSB) in transient absorption only reflects the excited electron population, as the density of the band edge for excited electron states is significantly smaller than the corresponding density of the hole states. In previous studies, an increase in the rate of the CdSe quantum dot GSB recovery can be clearly observed when the quantum dots are attached to electron acceptors while the kinetics remain the same when the quantum dots are attached to hole acceptors.[12,59] The transient absorption kinetics of CdSe quantum dots at the maximum bleach stay almost constant with the quantum dot/cluster assemblies, which indicates that no additional depopulation pathway for the excited electrons has been established (**Figure 2.4**). Considering that the time-resolved photoluminescence of the CdSe quantum dot/iron carbonyl cluster assemblies is quenched more rapidly than for pure CdSe quantum dots, it is concluded that efficient hole transfer from excited CdSe quantum dots to the iron clusters contribute to the enhanced hydrogen evolution activity. This finding is opposite to that which has been proposed previously for the CdSe quantum dot/$[Fe_2S_2(CO)_6]$ assembly.[25,40]

2.5. A g-C_3N_4/CdSe Quantum Dot/Iron Carbonyl Cluster Composite Photocatalytic Hydrogen Evolution System

In paper II, a g−C_3N_4/CdSe quantum dot/$[Fe_2S_2(CO)_6]$ composite was successfully constructed. This composite corresponds to a Type II heterojunction and shows excellent stability for photocatalytic hydrogen production. The structure, chemical composition, and optical properties of the prepared samples were investigated via a series of characterization techniques, and the ability of the assembly to catalyze proton reduction to form hydrogen gas was studied. With visible light irradiation for 4 hours, the total H_2 production amount of the g−C_3N_4/CdSe quantum dot/$[Fe_2S_2(CO)_6]$ assembly was 24-fold as high as the corresponding CdSe/$[Fe_2S_2(CO)_6]$ assembly in the absence of g-C_3N_4, and significantly higher than either the CdSe quantum dots or g−C_3N_4 alone. Transient absorption and time-resolved photoluminescence spectroscopies have been used to investigate the charge carrier transfer dynamics in the g−C_3N_4/CdSe quantum dot/$[Fe_2S_2(CO)_6]$ assembly system. The spectroscopic results indicate efficient hole transfer from the valence band of the excited CdSe quantum dots to the molecular iron carbonyl clusters and from the defect state of the quantum dots to g−C_3N_4 in the g−C_3N_4/CdSe quantum dot/$[Fe_2S_2(CO)_6]$ composite, which significantly inhibits the recombination of photogenerated charge carriers in CdSe quantum dots and boosts the photocatalytic activity and stability for hydrogen evolution. At the same

time, the energy transfer from g−C_3N_4 to CdSe quantum dot/[$Fe_2S_2(CO)_6$] assembly with a time constant of 0.7 ns also contributed to the charge transfer process. See paper II for further details.

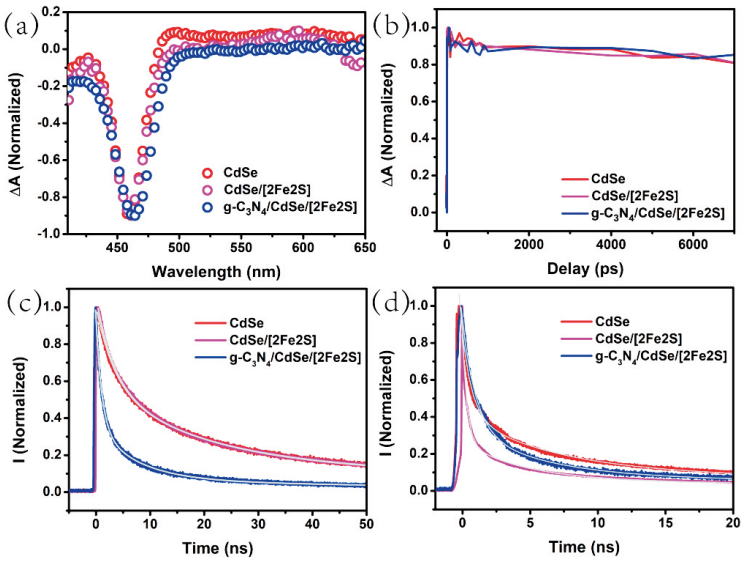

Figure 2.4. (a) Transient absorption spectra at 10 ps after excitation at 400 nm; (b) Transient absorption kinetics at the minimum bleach; (c) The time–resolved photoluminescence decay (λ> 610nm); (d) The time–resolved photoluminescence decay (470nm<λ<600nm) of pure CdSe quantum dots, CdSe quantum dot/[$Fe_2S_2(CO)_6$] assembly and g−C_3N_4/CdSe quantum dot/[$Fe_2S_2(CO)_6$] composite.[60]

2.6. Summary

The construction of assemblies of CdSe quantum dots with iron carbonyl clusters gives water soluble catalysts with enhanced activity for the photocatalytic hydrogen evolution reaction. Hole transfer is the dominant process in the two CdSe quantum dot/iron complex assemblies that have been studied, rather than electron transfer from the conduction band of the semiconductor to the iron complex, as has been proposed previously. However, the stabilities and efficiencies of such semiconductor/biomimetic systems are poor. Deposition of the quantum dot/iron carbonyl cluster assemblies on graphitic carbon nitride leads to further enhanced photocatalytic hydrogen evolution and increased stability. Graphitic carbon nitride can be an excellent support for nanoparticle photocatalysts.

Chapter 3: Photoinduced Hydrogen Evolution using Co(II) Compounds (Paper III)

3.1. Cobalt Materials and Complexes in Artificial Photosynthesis

Cobalt is one of the first row transition metals with the greatest ability to support multiple oxidation states, occupy both high and low spin electronic states, and adopt multiple coordination geometries depending on its surrounding ligands.[61] The entity that achieves water splitting in photosynthesis is the oxygen evolving complex (OEC), an Mn_4Ca oxo cluster complex that resides in photosystem II (PSII). An artificial OEC composed of cobalt, oxygen, and phosphate (**3.1**, **Figure 3.1**) that self-assembles upon the oxidation of Co^{2+} to Co^{3+} ion in aqueous solution has been reported.[62,63] This cobalt compound consists of edge-sharing CoO_6 octahedra.[64,65] The average size of the molecular cobaltate cluster is seven atoms and a nearly identical structural congener of the OEC of PSII, as schematically illustrated in **Figure 3.1**a. The artificial Co-OEC catalyzes water oxidation at neutral pH with high activity.[66] A number of effective mononuclear cobalt complexes have also been developed as water oxidation catalysts.[67] For example, a cobalt(II) center was inserted into the tetrapodal pentadentate ligand, 2,6-(bis(bis-2-pyridyl)- methoxymethane)pyridine (PY5), and it was found that the complex $[Co(II)(PY5)(OH_2)]^{2+}$ (**3.2**) functions as a remarkably active water oxidation catalyst.[68]

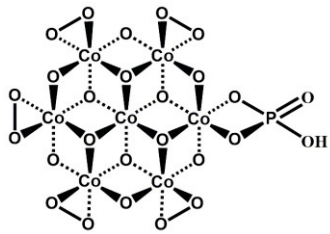

3.1

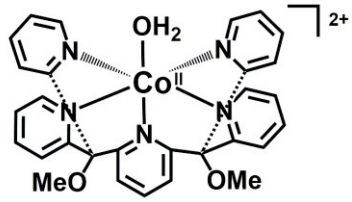

3.2

Figure 3.1. The artificial Co-OEC cubane structure **3.1** rotated by 45° to more clearly show edge sharing octahedra. The alkali metal ions, which are not shown, likely reside above the 3-fold triangle defined by the μ-bridging oxygens; the water oxidation catalyst $[Co(II)(Py5)(OH_2)]^{2+}$ (**3.2**).

3.2. Cobalt Complexes with Pentadentate Ligands for Hydrogen Evolution Reaction

In addition to water oxidation catalysis, molecular cobalt complexes have also been intensively studied because of their promise as electro- and photocatalysts for the hydrogen evolution reaction.[69,70] **Figure 3.2** presents a series of Co complexes with pentadentate ligands reported by various research groups. Their redox potentials and photocatalytic properties are summarized in **Table 3.1** and **Table 3.2**, respectively. The related discussions are introduced in the following sections.

In 2011, Chang, Long and coworkers reported a series of Co(II) complexes coordinated with pentapyridyl ligands as catalysts for (photo)electrochemical production of H_2 in aqueous solutions (**3.3a–c**, **Figure 3.2**).[71-73] The neutral pentapyridyl groups and the cationic nature of their metal complexes afford water solubility and stability to complexes **3.3a**–**3c**.[72] The electron withdrawing trifluoromethyl ($–CF_3$) group of **3.3b** led to a 0.19 V anodic shift to –1.28 V (vs. Fc^+/Fc) for the $Co^{II/I}$ redox potential compared with complex **3.3a**.[72] In 2013, Chang, Long and coworkers reported the Co(II) complexes **3.4a** and **3.4b** that were designed to investigate the effects of (potentially) redox-active bpy ligands on electrocatalytic and photocatalytic proton reduction.[73] Both **3.4a** and **3.4b** showed more positive redox potentials for the $Co^{II/I}$ event than **3.3a**, indicating the stabilization of low-valent Co(I) species.[73] In 2015, another series of Co(II) complexes **3.5a**–**3.5d** with redox-active pyrazines ligands were investigated.[74,75] The $Co^{II/I}$ potential anodic shifts in CH_3CN of 0.25, 0.17, 0.29, and 0.57 V (vs. Fc^+/Fc) were observed for **3.5a**–**3.5d**, respectively, compared with **3.3a**. The electrocatalytic HER showed that **3.5b** was the most active catalyst among **3.5a**–**3.5d**,[74,75] while the TONs of **3.5b** were far lower than for complexes **3.4a** and **3.4b** (**Table 3.2**). This indicated that positively shifted potentials for the $Co^{II/I}$ couple may lead to efficient hydrogen evolution activity. The similar Co(II) complexes

3.4c,[76] **3.6a**[76] and **3.6b**[77] were reported with three different pentadentate ligands (**Figure 3.2**). The observed $Co^{II/I}$ redox potentials for these three complexes were found to be similar to those reported by Chang (**Table 3.1**).

In 2012, Zhao and coworkers reported the synthesis and H_2 production activity of Co(II) complex **3.7a** of the pentadentate ligand DPA-Bpy (**Figure 3.2**).[78,79] In order to investigate the electronic effects of the ligand scaffold and in an effort to improve the catalytic properties of **3.7a** for H_2 evolution, they replaced the pyridyl substituents in DPA-Bpy with more basic and conjugated isoquinoline groups to yield the new Co(II) complex **3.7b** (**Figure 3.2**).[80] Electrocatalytic H_2 production by **3.7b** indicated a significant activity improvement over **3.7a** with a lower over-potential, and higher TON and TOF under neutral pH, possibly resulting from a more stable low-valent Co center.[80] In 2014, Wang and coworkers reported Co(III) complexes **3.8a**–**3.8c** based on the pentadentate ligand N4Py (**Figure 3.2**) and studied the photocatalytic hydrogen evolution effected by these complexes.[81] These investigators reported that the nature of the monodentate ligand in the apical position of **3.8** results in different redox potentials for the $Co^{III/II}$ and $Co^{II/I}$ peaks (**Table 3.1**). Therefore, Wang and coworkers inferred an HER mechanism that involved the decoordination of one of the pyridyl groups of the pentadentate ligand. Subsequently, the groups of Blackman, Collomb, and coworkers reported the synthesis, characterization, and H_2 production activity of Co(III) complexes **3.8c**–**3.8h** of the pentadentate ligand containing various monodentate ligands (**Figure 3.2**).[82]

Another four Co(II) complexes, **3.9a**–**3.9d**, containing a tripyridine–diamine type pentadentate ligand, were reported by Sun and co-workers as catalysts for electrocatalytic hydrogen reduction in neutral solution.[83] The $Co^{II/I}$ redox potentials for **3.9a**–**3.9d** in THF were calculated to be − 1.69 V, − 1.78 V, − 1.66 V and − 1.80 V vs. Fc^+/Fc, respectively. In 2015, Verani and co-workers investigated the Co(II) complexes **3.10** and **3.11** with different types of tripyridine–diamine ligands for electrocatalytic HER.[84] The cathodic shifts were observed for both complexes at potentials of the $Co^{II/I}$ peak (**3.10**: –1.99 V; **3.11**: –1.92 V vs. Fc+/Fc), comparable to the observations for **3.9a-3.9d** (**Table 3.1**).

The above discussion has demonstrated that the efficient electro- and photocatalytic HER activity of Co(II) complexes can be achieved through ligand modifications to generate positively shifted potentials of the $Co^{II/I}$ redox couple. The ligand modifications include changing the electronic properties, changing the denticity, and/or incorporating a redox-active motif. It was decided to further investigate the influence of variations in stereoelectronic effects within the N4Py ligand framework. Two features were investigated: (i) the hydrogen evolution efficiency of Co(II) derivatives of N4Py-like ligands (as opposed to analogous Co(III)(N4Py) complexes) (ii) the stereoelectronic effects of substituting pyridyl moieties in the ligand framework with other nitrogen-donor moieties. Thus, the

three Co(II) complexes **3.12**–**3.14** of the pentadentate ligands based on the N4Py framework, where one or two terminal pyridyl substituents have been replaced by quinoline or N-methylbenzimidazolyl moieties, were studied as hydrogen evolution catalysts.[85] The $Co^{II/I}$ redox potentials for **3.12**–**3.14** in CH_3CN were measured to be − 1.47 V, − 1.73 V and − 1.64 V vs. Fc+/Fc, respectively. (**Table 3.1**). The potential for **3.12**, in particular, is positively shifted relative to those for analogous N4Py complexes (**3.9**, **Table 3.1**)

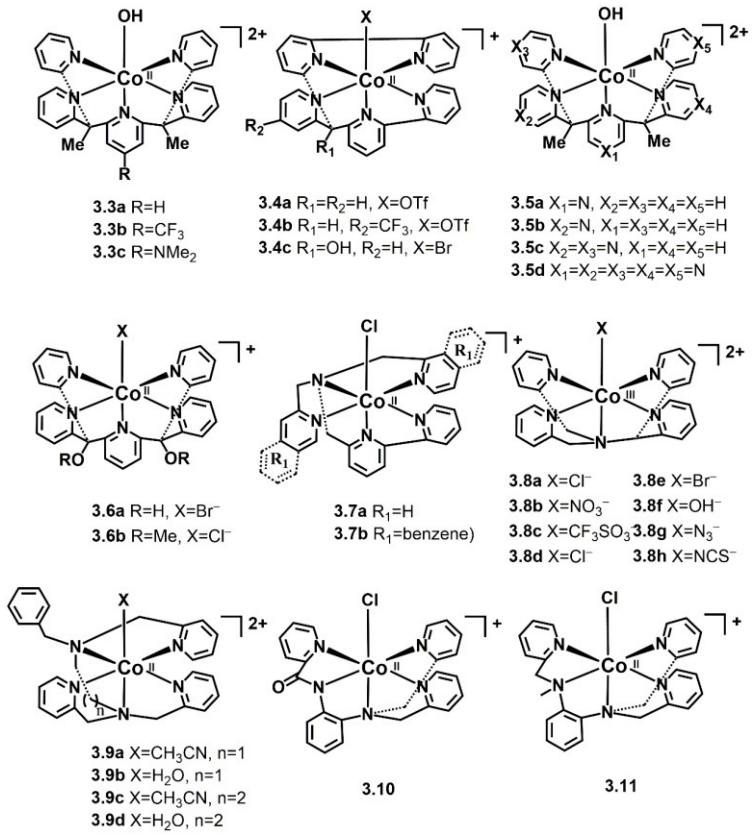

Figure 3.2. Pentadentate-based ligands and their corresponding cobalt complexes.

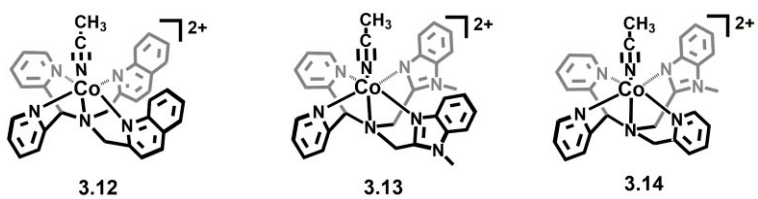

Figure 3.3. The pentadentate-based ligands and their corresponding Co(II) complexes studied in the present work.

Table 3.1. Experimental redox potentials of Co complexes with pentadentate ligands.[a]

Cat.	Electrolyte	$Co^{II/II}$	$Co^{II/I}$	Ref.
3.3a	CH_3CN (0.1 M nBu_4NPF_6)	0.24 V vs. Fc+/Fc	− 1.47 V vs. Fc+/Fc	[72]
3.3b	CH_3CN (0.1 M nBu_4NPF_6)	0.34 V vs. Fc+/Fc	− 1.28 V vs. Fc+/Fc	[72]
3.4a	CH_3CN (0.1 M nBu_4NPF_6)	0.235 V vs. Fc+/Fc	− 1.2 V vs. Fc+/Fc	[73]
3.4b	CH_3CN (0.1 M nBu_4NPF_6)	0.31 V[b] vs. Fc+/Fc	− 1.14 V[b] vs. Fc+/Fc	[73]
3.5a	CH_3CN (0.1 M nBu_4NPF_6)	0.32 V vs. Fc+/Fc	− 1.22 V vs. Fc+/Fc	[74]
3.5b	CH_3CN (0.1 M nBu_4NPF_6)	0.27 V vs. Fc+/Fc	− 1.30 V vs. Fc+/Fc	[74]
3.5c	CH_3CN (0.1 M nBu_4NPF_6)	0.35 V vs. Fc+/Fc	− 1.18 V vs. Fc+/Fc	[74]
3.5d	CH_3CN (0.1 M nBu_4NPF_6)	0.55 V vs. Fc+/Fc	− 0.90 V vs. Fc+/Fc	[75]
3.6b	CH_3CN (0.1 M $LiClO_4$)	0.09 V[b] vs. Fc+/Fc	− 1.71 V[b] vs. Fc+/Fc	[77]
3.8a	CH_3CN (0.1 M nBu_4NPF_6)	− 0.26 V[b] vs. Fc+/Fc	− 1.86 V[b] vs. Fc+/Fc	[81]
3.8b	CH_3CN (0.1 M nBu_4NPF_6)	− 0.45 V[b] vs. Fc+/Fc	− 1.65 V[b] vs. Fc+/Fc	[81]
3.8d	CH_3CN (0.1 M nBu_4NPF_6)	− 0.28 V[c] vs. Fc+/Fc	− 1.79 V[c] vs. Fc+/Fc	[82]
3.8e	CH_3CN (0.1 M nBu_4NPF_6)	− 0.19 V[c] vs. Fc+/Fc	− 1.72 V[c] vs. Fc+/Fc	[82]
3.8g	CH_3CN (0.1 M nBu_4NPF_6)	− 0.86 V[d] vs. Fc+/Fc	−	[82]
3.8h	CH_3CN (0.1 M nBu_4NPF_6)	− 0.29 V[c] vs. Fc+/Fc	− 1.70 V[c] vs. Fc+/Fc	[82]
3.9a	THF (0.1 M nBu_4NPF_6)	− 0.01 V vs. Fc+/Fc	− 1.69 V vs. Fc+/Fc	[83]
3.9b	THF (0.1 M nBu_4NPF_6)	−	− 1.78 V vs. Fc+/Fc	[83]
3.9c	THF (0.1 M nBu_4NPF_6)	−	− 1.66 V vs. Fc+/Fc	[83]
3.9d	THF (0.1 M nBu_4NPF_6)	−	− 1.80 V vs. Fc+/Fc	[83]
3.10	CH_3CN (0.1 M nBu_4NPF_6)	− 0.69 V vs. Fc+/Fc	− 1.99 V vs. Fc+/Fc	[84]
3.11	CH_3CN (0.1 M nBu_4NPF_6)	− 0.02 V vs. Fc+/Fc	− 1.92 V vs. Fc+/Fc	[84]
3.12	CH_3CN (0.1 M nBu_4NPF_6)	0.59 V[e] vs. Fc+/Fc	− 1.47 V[e] vs. Fc+/Fc	[85] (*this work*)
3.13	CH_3CN (0.1 M nBu_4NPF_6)	0.445 V[e] vs. Fc+/Fc	− 1.73 V[e] vs. Fc+/Fc	[85](*this work*)
3.14	CH_3CN (0.1 M nBu_4NPF_6)	0.195 V[e] vs. Fc+/Fc	− 1.64 V[e] vs. Fc+/Fc	[85] (*this work*)

[a] E(Fc+/Fc) = 0.64 V vs. SHE. [b] Converted from E(SCE) = 0.24 V vs. SHE. [c] Converted from E($Ag/AgNO_3$ (0.01 M in CH_3CN)) = 0.54 V vs. SHE. [d] E_{pc}. [e] $E_{1/2}$.

3.3. Photocatalytic Hydrogen Production and Mechanistic Study by Molecular Cobalt (II) Catalysts

In the presence of $[Ru(bpy)_3]^{2+}$ and ascorbic acid in 1.0 M phosphate buffer at pH 6, **3.3b** shows the highest photocatalytic water reduction activity among **3.3a-c**, with a TON of 300.[72] Under both electrocatalytic and photocatalytic conditions, the improved HER activity by **3.3b** demonstrates the electronic tuning with an electron withdrawing group (-CF_3) in the ligand scaffold as an efficient approach to modifying the activity of water reduction.[72] The TONs for photocatalytic H_2 evolution with **3.4a** and **3.4b** for 13 h were 1630 and 1390, respectively,[73] while the TONs decreased substantially under the same experimental conditions when pyridine units were replaced by pyrazine in the similar Co(II) complexes **3.5a-3.5d** (**Table 3.2**).[74]

Wang and coworkers reported that variation of the sixth monodentate ligand in the Co(III)(N4py) complexes **3.8a-3.8c** has a dramatic effect on the photocatalytic H_2 production in aqueous solutions,[81] while, on the other hand, Blackman, Collomb, and coworkers show that there is not much difference in the photocatalytic activity for H_2 production among complexes **3.8d-3.8h**.[82] Wang and coworkers found that a much higher amount of H_2 was achieved in NaCl solution than in Na_2SO_4 solution. This result contradicts the hypothesis that the formation of a Co(III)-H intermediate is the result of the dissociation of the chloride ligand, since the addition of NaCl is believed to stabilize the coordination of the chloride ligand. The result further suggests that there must be another reaction, such as decoordination of a pyridine group of the N4Py ligand, to account for the formation of Co(III)-H. The results of Wang and coworkers are similar to those that were obtained Polyansky and coworkers from pulse radiolysis and a DFT study of H_2 production by complex **3.6**.[86] However, Blackman, Collomb and coworkers suggest a different mechanism for H_2 production based on their studies of complexes **3.8d-3.8h** containing the same pentadentate ligand N4Py as in **3.8a-3.8c,** but with different counterion(s) (ClO_4^- for **3.8d-3.8h**).[82] The latter authors concluded from bulk electrolysis, UV-Vis, and EPR analysis of complexes **3.8d-3.8h** that although the monodentate ligands remain coordinated with the Co center in both the Co(III) complexes and their corresponding Co(II) forms formed by electrochemical reduction of the Co(III) complexes in CH_3CN solution, the Co(II) form that is produced through chemical reduction by ascorbic acid (H_2A) has a common formula of $[Co(II)(N4Py)(HA)]^+$. Electrochemical and UV-Vis characterization of corresponding Co(I) species indicates that loss of monodentate ligands occurs during the reduction of Co(II) to $[Co(I)]^+$. The photocatalytic H_2 evolution activities for **3.8d-3.8h** were found to be similar and independent of the nature of the apical monodentate ligands, indicating that during the entire course of hydrogen evolution catalysis, N4Py remains fully coordinated with the Co center.[82]

3.4. Photoinduced Hydrogen Evolution Catalyzed by New Co(II) Complexes of N5-donor Ligands

In paper III, the photocatalytic properties of Co(II) complexes **3.12-3.14** were studied using $[Ru(bpy)_3]^{2+}$ as photosensitizer and ascorbic acid as a sacrificial electron donor (**Table 3.2**). The three ligands are modifications of the N4Py ligand discussed above, where one or two pyridyl units have been replaced by other heteroaromatic nitrogen donor units. In the study included in this thesis, light-driven H_2 production with TONs in the range of 16–25 was determined for complexes **3.12-14**.[85]

Table 3.1. Photochemical hydrogen production properties of Co complexes with pentadentate ligands.

Cat.	Solvent	PS ($[Ru(bpy)_3]^{2+}$)	Reductant (H_2A)	[Cat]	pH	TON	Ref.
3.3a	1 M phosphate buffer	200μM	0.1 M	50μM	7	0.38	[72]
3.3b	1 M phosphate buffer	200μM	0.1 M	50μM	7	0.44	[72]
3.3c	1 M phosphate buffer	200μM	0.1 M	50μM	7	0.22	[72]
3.4a	H_2O	330μM	0.3 M	20μM	4	1630	[73]
3.4b	H_2O	330μM	0.3 M	20μM	4.5	1390	[73]
3.4c	H_2O	500μM	1 M	5μM	4.1	1380	[76]
3.5a	H_2O	330μM	0.3 M	20μM	5.5	190	[74]
3.5b	H_2O	330μM	0.3 M	20μM	5.5	450	[74]
3.5c	H_2O	330μM	0.3 M	20μM	5.5	170	[74]
3.6a	H_2O	500μM	1 M	5μM	4.1	1180	[76]
3.6b	1 M acetate buffer	500μM	0.1 M	50μM	4	187	[77]
3.8a	H_2O	100μM	0.1 M	50μM	4	0.14	[81]
3.8b	H_2O	100μM	0.1 M	50μM	4	0.03	[81]
3.8c	H_2O	100μM	0.1 M	50μM	4	0.10	[81]
3.8d	H_2O	500μM	1.1 M	100μM	4	59	[82]
3.8e	H_2O	500μM	1.1 M	100μM	4	63	[82]
3.8g	H_2O	500μM	1.1 M	100μM	4	59	[82]
3.8h	H_2O	500μM	1.1 M	100μM	4	61	[82]
3.12	H_2O/CH_3CN (1:1 v/v)	130μM	0.125 M	130μM	4	25.2	[85] (*this work*)
3.13	H_2O/CH_3CN (1:1 v/v)	130μM	0.125 M	130μM	4	19.7	[85] (*this work*)
3.14	H_2O/CH_3CN (1:1 v/v)	130μM	0.125 M	130μM	4	16.1	[85] (*this work*)

The photochemical mechanism, as revealed by nanosecond time-resolved transient absorption spectroscopy, involves reaction of the excited sensitizer with ascorbic acid to yield $[Ru(bpy)_3]^+$ as a primary photogenerated reductant, capable of electron transfer to the cobalt catalyst(s) (Figure 3.4). Figure 3.4a and 3.4b show examples of the ns TA data in the absence and presence of catalyst **3.13**, respectively. The emergence of $[Ru(II)(bpy)_2(bpy)\bullet^-]^+$, due to reductive quenching of the ^{3}MLCT state of the photosensitizer, is characterized by a time constant of 120 ps irrespective of the presence of a catalyst (Figure 3.4c). At about 600 ns the initial spectral changes due to formation of $[Ru(II)(bpy)_2(bpy)\bullet^-]^+$ are complete and the resultant differential absorption signal decays to zero within 400 μs (Figure 3.4a-c). In the absence of a Co(II) catalyst, the experimentally observed time constants are 9 and 54 μs. A bi-exponential decay in the absence of a catalyst was also observed by Blackman et al.[82] The authors rationalized this finding by charge recombination between $[Ru(II)(bpy)_2(bpy)\bullet^-]^+$ and different oxidized forms of ascorbate (i.e. HA• radical and the dehydroascorbic acid A).[82] In the presence of a catalyst, the decay of $[Ru(II)(bpy)_2(bpy)\bullet^-]^+$ becomes slightly faster, i.e. the characteristic time-constants are determined to be 5 and 30 μs for catalyst **3.13** (Figure 3.4d). This finding points to the fact that intermolecular electron transfer from $[Ru(II)(bpy)_2(bpy)\bullet^-]^+$ to the catalyst presents an additional decay channel for the reduced photosensitizer.

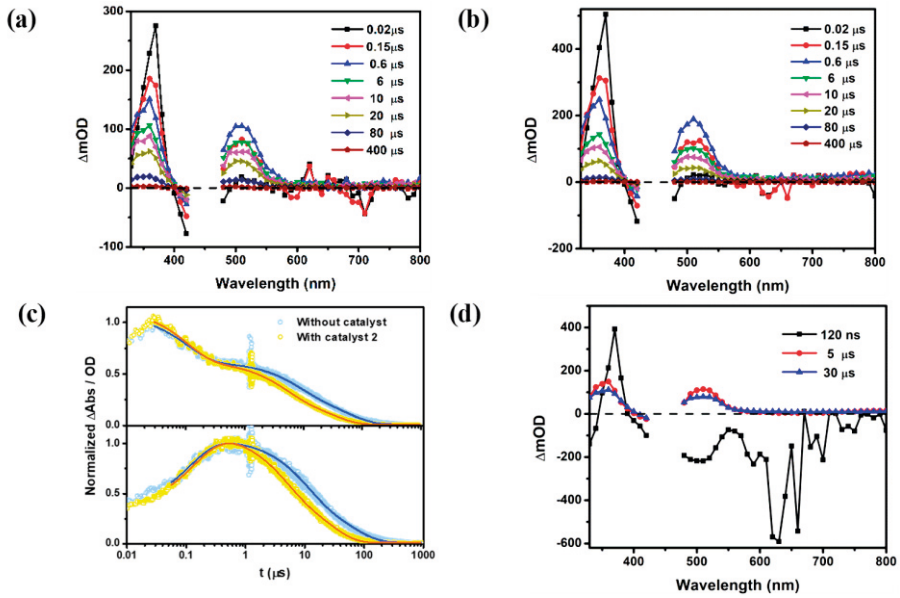

Figure 3.4. Nanosecond transient absorption (TA) spectra of the solution containing 0.13 mM $[Ru(bpy)_3]^{2+}$, 110 mM ascorbic acid and (a) without a Co(II) catalyst and (b) with 0.13 mM catalyst 2 upon excitation at 450 nm in aerated water/acetonitrile mixture (1:1 v/v) at pH 4. (c) Comparison of the normalized kinetics with the corresponding fit at 360 (upper) and 500 nm (bottom). (d) Global fit results of the ns TA data shown in (b).

On the basis of the photophysical data and previous photophysical and computational studies on other photocatalytic systems for hydrogen evolution involving related molecular Co(II) and Co(III) catalysts,[78,82,86-94] it is proposed that the photocatalytic cycle begins with the reduction of $*[Ru(bpy)_3]^{2+}$ by ascorbate to afford the reduced state $[Ru(bpy)_3]^{+}$ and the neutral radical HA• (Figure 3.5). The HA• species is known to deprotonate easily to form the radical anion A•− that disproportionates in acidic aqueous solution to give HA− (A^{2-}) and two-electron oxidized dehydroascorbic acid A. Reduced $[Ru(bpy)_3]^{+}$ possesses a sufficiently negative potential to reduce the Co(II) catalyst to the Co(I) oxidation state, and that reduced species enters the catalytic cycle for H_2 evolution (Figure 3.5). The reduced Co(I) complex can react with a proton under acidic conditions to generate a Co(III) hydride complex.[82] As previously discussed, studies on $[Co(III)(N4Py)(X)]^{n+}$ by Wang and coworkers[81] and Blackman, Collomb and coworkers[82] gave conflicting results – Wang and coworkers obtained results that suggest partial decoordination of the pentadentate ligand in the formation of the Co(III)-hydride complex, whereas the catalytic results obtained by the latter group strongly implicated dissociation of the apical ligand to form a five-coordinate Co(I) complex that can react with a proton. As discussed by Blackman, Collomb and coworkers[82] the resultant six-coordinate Co(III) hydride complex may react in different ways. One possibility is a reaction with a second Co(III) hydride complex and homolytic cleavage of the Co(III)-H bonds to generate H_2 and the

corresponding Co(II) species which in turn may react with HA− to form [Co(II)(AH)(N5-ligand)]$^{+}$, as schematically depicted in the catalytic cycle in Figure 3.5. A second possibility (not depicted) is the reaction of the Co(III) hydride complex with a proton (oxonium ion) to generate H_2 via heterolytic cleavage of the Co(III)-H bond; however, there should be a significant electrostatic barrier for the initial association of the two cations. The relatively low activity of hydrogen production may be explained by the low stability of the Co(I) species that are formed in the catalytic systems.

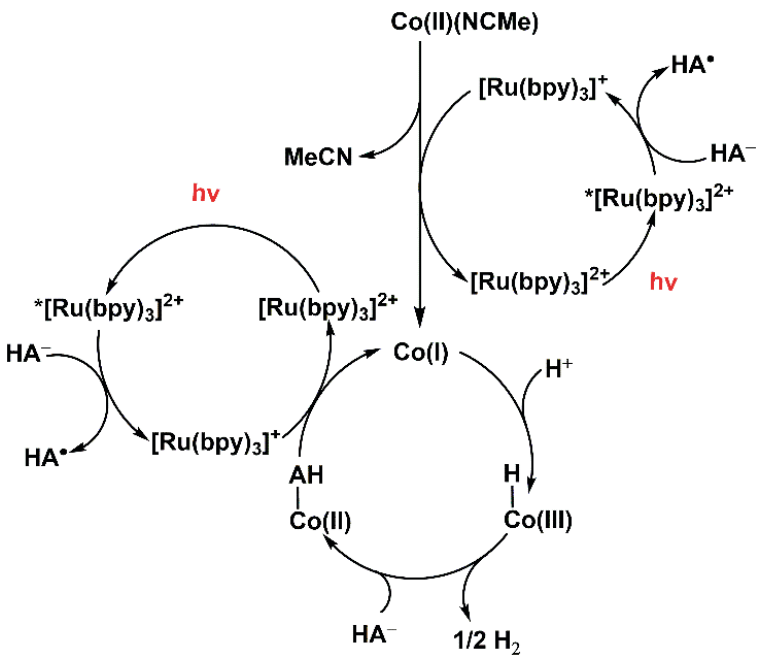

Figure 3.5. Schematic summary of the primary photochemical processes and a possible catalytic HER cycle occurring upon light irradiation of the photolysis mixture containing $[Ru(bpy)_3]^{2+}$, cobalt catalyst (**3.12-3.14**), and ascorbic acid（bpy=2,2'bipyridine).

3.5 Summary

The effective ligand fields exerted by the ligands in a series of related cobalt(II) complexes affect the Lewis basicities of the cobalt ions and hence the effectiveness of the complexes as catalysts for light-driven HER. The catalytic activity appears to be limited by the low stabilities of the Co(I) species that are formed in the photocatalytic processes.

The hydrogen evolution activity of cobalt molecular catalysts can be modulated by ligand modification, including variation in steric and electronic constraints and the

introduction of redox-active groups (so called “non-innocent ligands”). During catalytic HER, the generation of a vacant coordination site at the Co center is an important step that needs to be facilitated and better studied. The robustness of Co catalysts under catalytic conditions is another major issue, and strategies for preventing the dissociation of Co ions during catalysis may be the key to improving catalyst stability. The catalytic efficiencies of the three new Co(II) complexes that have been studied are low. Efforts to stabilize low valent Co(I) species under catalytic conditions may need to be considered for the enhancement catalyst operation and stability. For example, preventing the formation of metallacycle by-products via ligand intramolecular metalation may decrease the deactivation of cobalt catalysts during hydrogen production.[70,95]

Chapter 4: Molybdenum Sulfides as Catalysts for Hydrogen Evolution Reactions (Paper IV)

Extensive efforts have been made to develop efficient electro- and photocatalysts for the hydrogen evolution reaction that are based on earth-abundant elements and may be used in large-scale applications.[96-98] Molybdenum sulfides are attractive noble-metal-free catalysts that show an outstanding activity as catalysts for electrocatalytic hydrogen production. Crystalline molybdenum disulfide (MoS_2) shows a typical layered sandwich-like structure held by weak van der Waals interactions.[99] However, only the edges of the layered solid state structure of MoS_2 act as active sites, while the basal planes are inert (**Figure 4.1**).[100] Many strategies have been explored to increase the exposure of active edge sites and improve the catalytic activity of crystalline MoS_2.[101,102] Various MoS_2-based nanostructures, including single-/few-layer nanosheets,[103] nanodots,[104] nanoflowers,[105] and quantum dots[106] have been prepared by morphology control in order to maximize the number of catalytically active sites. Generation of defects or element doping have also been employed as methods to activate the basal planes of MoS_2.[107,108] In addition to studies on crystalline molybdenum disulfide, molecular molybdenum sulfide clusters and amorphous molybdenum sulfides (MoS_x; x =2–3) have been synthesized and their hydrogen evolution reaction activities have been investigated.[109-114]

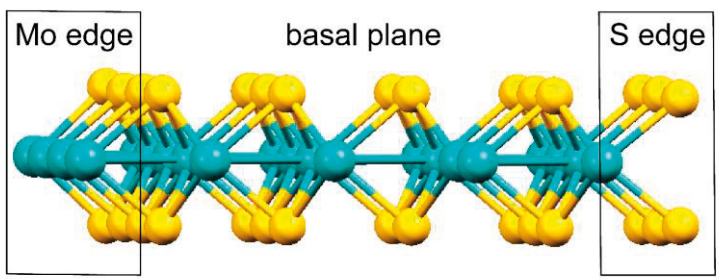

Figure 4.1. monolayer of a perfect triatomic MoS_2, Color code for ball-and-stick models: Mo, turquoise; S, yellow.

4.1. Molybdenum Sulfides as Electrocatalysts for the Hydrogen Evolution Reaction

The mechanism(s) of HER catalysis by molybdenum sulfides (e.g. crystalline MoS_2 and amorphous MoS_x) is still not well understood, and the real active sites need to be further confirmed. Molecular clusters are considered to be suitable active site models for molybdenum sulfides that can be used to investigate mechanisms of reactions catalyzed by such solids.[115] For the electrocatalytic HER, catalysts consisting of heterogeneous systems based on molecular $[Mo_xS_y]$ clusters have been studied because of their richness in unsaturated Mo-S coordination sites, which is characteristic of the active MoS_2 edge.[112,116,117]

Chorkendorff and coworkers reported the molecular MoS_x complex **4.1** (Figure 4.2), consisting of an incomplete cubane-type $[Mo_3S_4]^{4+}$ cluster, to possess sites similar to the edge sites of crystalline MoS_2.[117] After deposition on a FTO electrode, the electrocatalytic HER activity of the $[Mo_3S_4]^{4+}$ cluster was comparable with that of the edge sites of MoS_2 over a period of one hour, and then slow desorption from the electrode due to the hydrophilicity of the clusters was observed. Chang and coworkers identified the Mo^{IV}−disulfide complex $[(PY5Me_2)MoS_2]^{2+}$ **4.2** (**Figure 4.2**), and this complex exhibited considerably higher stability and larger TOFs than **4.1** in electrocatalytic HER under the same experimental conditions.[118]

Two more typical thiomolybdate clusters, trinuclear $[Mo_3S_{13}]^{2-}$ **4.3**[116] and dinuclear $[Mo_2S_{12}]^{2-}$ **4.4**,[112] have been investigated as HER electrocatalysts. High electrocatalytic activity was found for complex **4.3** (deposited on carbon electrodes) under acidic conditions, and for **4.4** deposited on fluoride-doped tin oxide (FTO) substrates.[112,116] Yaghi and coworkers[119] have prepared a series of $[Mo_3S_7]$-based metal−organic sulfides (MOS) in which various organic linkers connect the trimolybdenum clusters through strong chemical bonds into well-defined structures such as dimers and chains. These MOS compounds were found to be excellent catalysts for electrocatalytic hydrogen evolution when deposited on FTO electrodes. A 40-fold enhancement in turnover frequency was observed in MOS systems compared with the unlinked cluster. The periodic arrangement of clusters on the electrode with control over their distance, orientation, and density, explains the low overpotential of only 89 mV to achieve a current density of 10 mA cm^{-2} with the MOS systems.

4.2. Photocatalytic Hydrogen Production Catalysed by Molybdenum Sulfide Clusters

The thiomolybdate clusters $[Mo_3S_{13}]^{2-}$ (**4.3**) and $[Mo_2S_{12}]^{2-}$ (**4.4**) have been investigated as catalysts for light-driven hydrogen evolution in homogeneous systems and were found to produce remarkable turnover numbers (TON).[120-122] The efficiency of H_2 production by the metal sulfide clusters was found to be influenced by the solvents and the ratios of solvents in solvent mixtures. Streb and coworkers suggest that a stepwise exchange of the terminal disulfido ligands with aquo ligands is a key step when the $[Mo_3S_{13}]^{2-}$ cluster is used under photocatalytic conditions, and the H_2 evolution activity was found to be the highest in methanol/water (10:1 v/v) for this cluster.[120] However, when $[Mo_2S_{12}]^{2-}$ was used as a catalyst under the same experimental conditions, it was found that the TON of the photocatalytic hydrogen evolution was optimal in pure methanol rather than a methanol/water mixture.[122] Streb and coworkers suggest that the charge transfer from the photosensitizer ($[Ru(bpy)_3]^{2+}$) to the $[Mo_3]$ catalysts may play a crucial role in controlling homogeneous light-driven hydrogen evolution activity for molybdenum sulfide cluster systems. The charge transfer rate from $[Ru(bpy)_3]^{2+}$ to

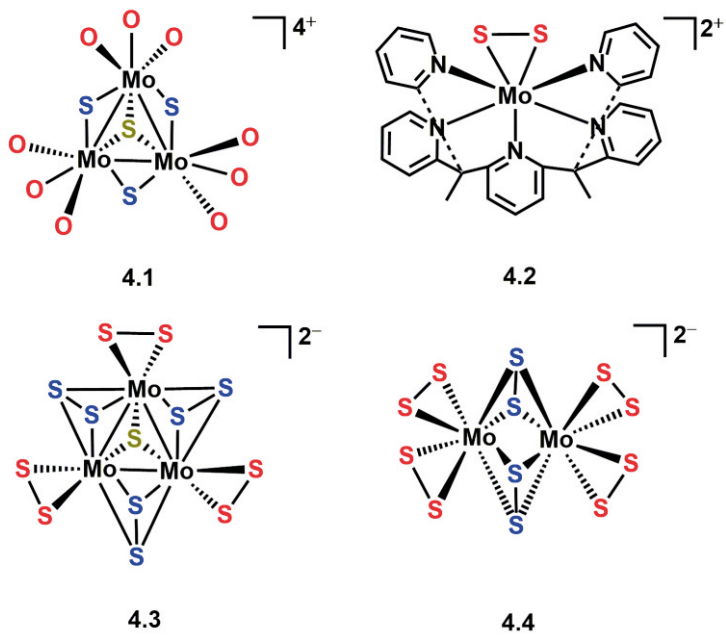

Figure 4.2. Molecular structures of $[Mo_3S_4]^{4+}$ (**4.1**, O from water ligands), $[(PY5Me_2)MoS_2]^{2+}$ (**4.2**), $[Mo_3S_{13}]^{2-}$(**4.3**) and $[Mo_2S_{12}]^{2-}$(**4.4**), highlighting the different arrangements of the sulfur anions around the molybdenum cations : red (terminal disulfides), blue (bridging disulfides) and dark yellow (apical sulfide).

[Mo_3], [Mo_3]–Cl or [Mo_3]–Br were explored in MeOH:H_2O (10:1, v/v) by measuring the Stern–Volmer plots, which indicated that the $[Ru(bpy)_3]^{2+}$-^{3}MLCT emission depends on the catalyst concentration. Higher quenching efficiency was observed for [Mo_3] compared with [Mo_3]–Cl or [Mo_3]–Br in the same concentration range. The measurements indicate that faster charge transfer from $[Ru(bpy)_3]^{2+}$ to [Mo_3] cluster occurs than that from $[Ru(bpy)_3]^{2+}$ to [Mo_3]–Cl or [Mo_3]–Br cluster.

4.3. Metal-organic Sulfides for Light-driven Hydrogen Evolution

Considering the excellent electrocatalytic HER properties exhibited by the metal-organic sulfides (MOS) studied by Yaghi and coworkers, it was decided to investigate the photocatalytic properties of these compounds. As described in paper IV, the photocatalytic hydrogen-generating activity of two different metal-organic sulfides - viz. MOS-1 and MOS-3, **Figure 4.3** - was studied in the presence of $[Ru(bpy)_3]^{2+}$, acting as a photosensitizer, and ascorbic acid acting as a sacrificial electron donor (**Table 4.1**). It was found that conditions similar to those used for $[Mo_3S_{13}]^{2-}$-catalyzed photocatalysis were optimal.[123] These conditions, and the conditions and results obtained in photocatalytic HER studies on related compounds, are listed in Table 4.1. Both of the molybdenum-based MOS show high efficiency for catalytic hydrogen production with maximum turnover numbers > 7900 for the dimer and > 9300 for the chain, respectively, based on [Mo_3 active sites]. The enhanced (photo)catalytic activity of these MOS compounds correlates with their observed electrochemical proton reduction

Table 4.1. Photochemical hydrogen production parameters for molybdenum sulfide clusters.[a]

Cat	Solvent	PS ($[Ru(bpy)_3]^{2+}$)	Reductant (H_2A)	[Cat]	pH	TON	Ref.
$[Mo_3S_{13}]^{2-}$	H_2O	20 μM	0.1 M	0.3 μM	6	2850	[120]
	H_2O/MeOH (1:1 v/v)	20 μM	0.1 M	0.3 μM	6	3950	[120]
	H_2O/MeOH (1:10 v/v)	20 μM	0.1 M	0.3 μM	6	23000	[120]
	H_2O/CH_3CN (1:9 v/v)	100 μM	0.1 M	2 μM	-	1570	[121]
$[Mo_2S_{12}]^{2-}$	H_2O	20 μM	0.01 M	0.5 μM	6	75	[122]
	MeOH	20 μM	0.01 M	0.5 μM	6	1630	[122]
	H_2O/MeOH (1:10 v/v)	20 μM	0.01 M	0.5 μM	6	900	[122]
$[Mo_3S_7Br_6]^{2-}$	H_2O/MeOH (1:10 v/v)	20 μM	0.1 M	0.3 μM	6	60	[120]
	H_2O/MeOH (1:4 v/v)	130 μM	0.125 M	0.5 μM	4	800	[123] (*this work*)
MOS-1	H_2O/MeOH (1:4 v/v)	130 μM	0.125 M	0.5 μM	4	7500	[123] (*this work*)
MOS-3	H_2O/MeOH (1:4 v/v)	130 μM	0.125 M	0.5 μM	4	9400	[123] (*this work*)
	MeOH	130 μM	0.125 M	0.5 μM	4	3245	[123] (*this work*)
	DMF	130 μM	0.125 M	0.5 μM	4	0	[123] (*this work*)
	H_2O/DMF (1:4 v/v)	130 μM	0.125 M	0.5 μM	4	0	[123] (*this work*)

a: MeOH:Methanol; DMF:Dimethylformamide.

activities when doped on FTO electrodes.[119] The efficiency of H_2 production by the MOS was found to be influenced by the solvents and the volume ratio of the solvent mixture, too. No traces of hydrogen were found for MOS-3 when the photocatalytic reaction was carried out in dimethylformamide or a dimethylformamide/water mixture (4:1 v/v). When the catalysis was carried out in methanol/water (4:1 v/v), the H_2 evolution activity of MOS-3 was found to be the highest, which is similar to results obtained Streb and coworkers.[120]

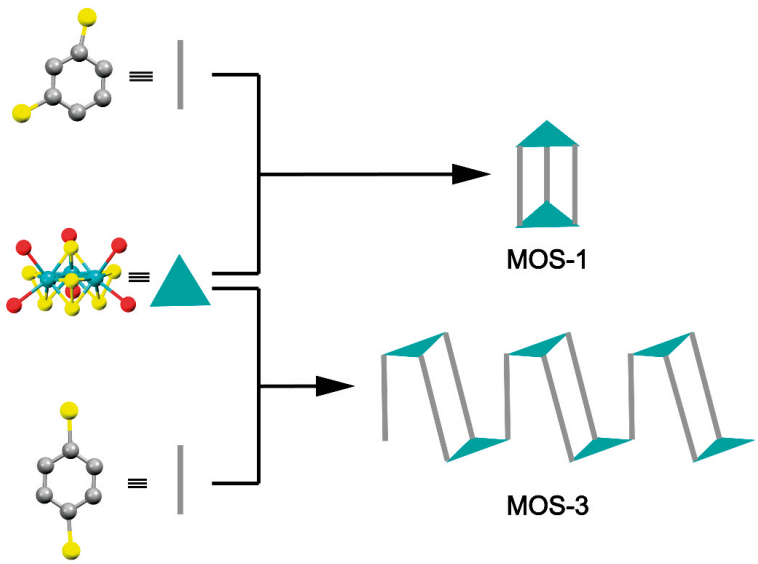

Figure 4.3. A schematic depiction of Mo_3S_7 clusters connected by the dithiolate linkers benzene-1,3-dithiolate (MOS-1) and benzene-1,4-dithiolate (MOS-3) into dimers and a chain. Color code for ball-and-stick models: Mo, turquoise; Br, red; S, yellow; C, gray.

4.4. Carrier Recombination Dynamics in Metal-organic Sulfides

In paper IV, time−resolved photoluminescence spectroscopy has been used to investigate the charge carrier transfer dynamics of the MOS compounds in different solvents.[123] Defect emission ($\lambda >$ 500 nm) of MOS-1 and MOS-3 in different, potentially coordinating, solvents/solvent mixtures (DMF, MeOH, MeOH/H_2O) have been studied and compared with that of $[Mo_3S_7Br_6]^{2-}$ (**Figure 4.4**). The MOS compounds show faster decay than $[Mo_3S_7Br_6]^{2-}$ regardless of the solvents used in this study (**Figure 4.4**a-c), which correlates with the observed photocatalytic hydrogen evolution activities (faster decay correlates with higher activity). An explanation for the faster decays in the MOS structures is that more efficient non-irradiative channels, *i.e.* more efficient charge carrier recombination, are introduced when the Mo_3 units are linked via thiolates. The solvent affects the

photocatalytic hydrogen evolution by molybdenum sulfide compounds,[120-123] as has been discussed above. The MOS compounds exhibited the most rapid photoluminescence decay in a MeOH/H_2O mixture, followed by pure methanol, and the slowest decay was observed in DMF (**Figure 4.4**d-f). When the MOS compounds or $[Mo_3S_7Br_6]^{2-}$ are dissolved in pure DMF solution, the solutions are uniformly clear; however, in pure methanol or a mixture of methanol and water, cloudy suspensions are gradually formed for all compounds. Streb and coworkers have obtained evidence that the terminal disulfides of $[Mo_3S_{13}]^{2-}$ may exchange with water,[120] and similar exchange may take place for the molybdenum sulfide compounds in this study, but this aspect needs to be investigated further.

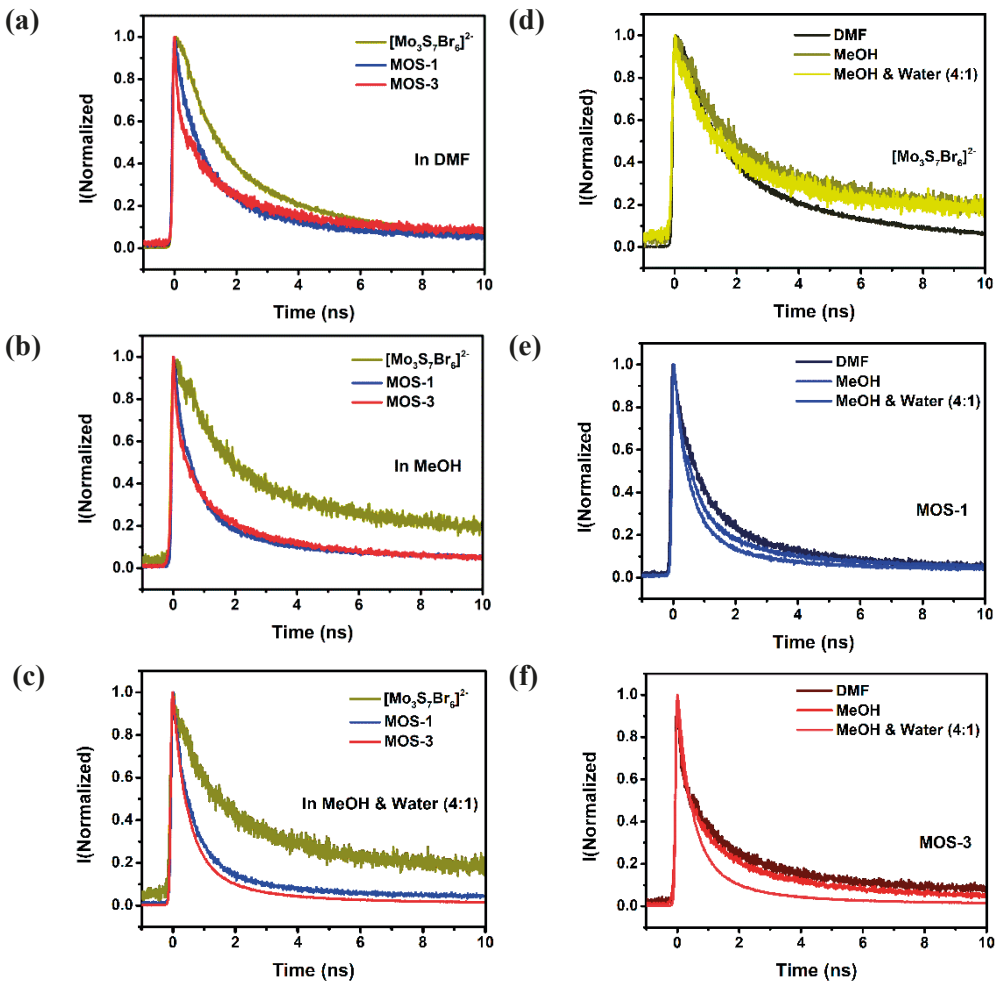

Figure 4.4. The time-resolved photoluminescence (TRPL) decay (λ> 500 nm) of different catalysts in different solvents : (a) DMF; (b) methanol; (c) MeOH/water (4:1 v/v); (d) starting cluster $[Mo_3S_7Br_6]^{2-}$; (e) MOS-1; (f) MOS-3.

4.4. Summary

The efficiency of HER catalysis may be improved by synthesizing molybdenum sulfide compounds/catalysts that maximize the number of catalytically active sites. Such systems include molecular, nanoparticulate, nanowire, mesoporous solid and amorphous film compounds/materials. Studies on molecular molybdenum sulfide clusters are suitable for understanding the mechanism(s) of photocatalytic hydrogen evolution effected by molybdenum sulfides. Construction of metal-organic sulfides through linking of molybdenum sulfide clusters via suitable ligands to form oligomeric or polymeric structures may lead to efficient electro- or photocatalytic catalysts for HER. This has been confirmed by the studies on MOS-1 and MOS-3 that are discussed above and in paper IV; these compounds exhibit excellent photocatalytic HER activities. A well-defined metal-organic sulfide may increase the charge carrier transfer rate and thus enhance hydrogen evolution activity. In addition, it may be easier to confirm the catalytically active sites in such materials, in comparison to relatively inhomogeneous molybdenum sulfides. Metal-organic sulfides provide a strategy to combine the advantages of both molecular and semiconductor molybdenum sulfide materials.

Further studies are needed to understand the mechanism(s) of photocatalytic hydrogen production by the molybdenum sulfide cluster-based systems studied in this thesis. Different techniques (e.g. femtosecond time-resolved transient absorption spectroscopy, density functional theory calculations) are needed to explore the physicochemical properties of the molybdenum sulfide clusters in different solvents.

Chapter 5: Conclusions and Outlooks

In this thesis, four different molecular or assembly-based light-driven hydrogen evolution systems have been developed and the mechanism(s) of the charge carrier transfer processes during photocatalytic hydrogen evolution have been investigated. The photocatalytic hydrogen-generating activity and stability of the different photocatalytic systems have been studied. Transient absorption and time-resolved photoluminescence spectroscopies have been used to investigate the charge carrier transfer dynamics in the catalytic systems. The close connection between photocatalytic hydrogen-generating activity and charge carrier transfer dynamics is the key component in this study. The construction of assemblies of CdSe quantum dots with molecular complexes (iron carbonyl clusters) gives water soluble catalysts with enhanced activity for the photocatalytic hydrogen evolution reaction. Hole transfer is the dominant process in the CdSe quantum dot/iron complex assemblies, rather than electron transfer from the conduction band of the semiconductor to the iron complex, as has been proposed previously. Graphitic carbon nitride can be an excellent support for nanoparticles in hydrogen production under light irradiation. The effective ligand fields exerted by the ligands in a series of related cobalt(II) complexes affect the Lewis basicities of the cobalt ions and hence the effectiveness of the complexes as catalysts for light-driven HER. The catalytic activity appears to be limited by the low stabilities of the Co(I) species that are formed in the photocatalytic processes. Time−resolved photoluminescence results indicate that the introduction of bridging thiolates between Mo_3 units in metal organic sulfide (MOS) materials generates efficient non-irradiative channels in the defect emission range and leads to more efficient HER catalysis.

However, there are still many challenges to construct an efficient photocatalytic system. Non-toxic metal semiconductor photosensitizers should be developed and studied. Photocatalytic hydrogen production systems that function in neutral aqueous solution need to be explored. Among the molecular complexes studied in this thesis, the lifetimes of the photocatalytic reactions were short - from 30 mins up to several hours, after which decomposition was observed. Significant improvements in the stability of the catalysts are required for future applications. The decomposition of molecular metal complexes into nanoparticles during catalysis is certainly possible and has been confirmed.[124-126]

Appendix: Experimental Methods

Photocatalytic H_2 Production

The light-driven hydrogen evolution experiments were performed at room temperature. Reactants were added into a homemade photocatalysis reactor. The reaction was carried out under irradiation by a 300 W Xenon lamp (Excelitas Technologies, PE300BFM). The hydrogen product was collected by airtight syringe in the head space of the reactor and then monitored by gas chromatography using a molecular sieve column (5 Å), thermal conductivity detector, and argon carrier gas (**Figure A.1**).

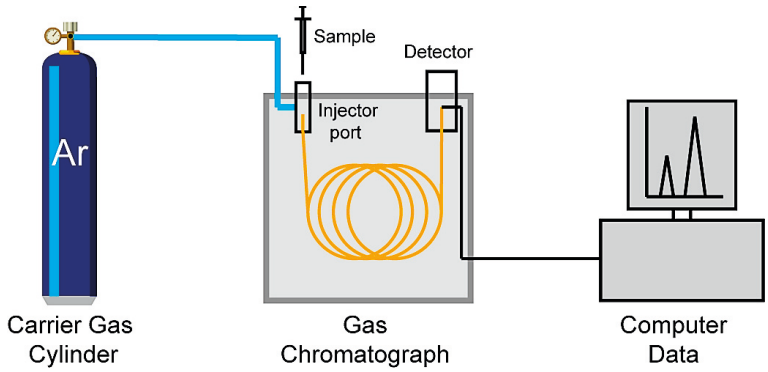

Figure A.1. The measurement procss of hydrogen production.

After the collection of raw data for H_2 production, the data were compared with external standard data to obtain the real amount of hydrogen production. In a standard calibration method, the absolute pure H_2 response is plotted against the known amount to create a calibration curve (**Figure A.2**).

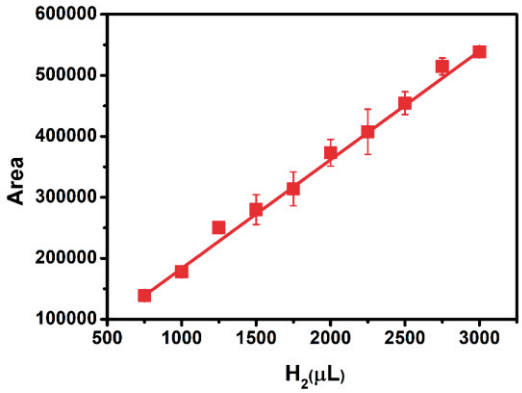

Figure A.2. Standard H_2 calibration plot (pure H_2 vs hydrogen peak area in GC).

Time-Resolved Spectroscopy

The semiconductors that have been studied, e.g. quantum dots or assemblies containing quantum dots, g-C_3N_4 and molybdenum sulfide metal-organic polymers, emit photoluminescence. This enables studies of the excited-state dynamics in these materials by time-resolved photoluminescence (TRPL) spectroscopy. Two different TRPL spectroscopic methods were used: time-correlated single photon counting (TCSPC) and a streak camera. The two techniques have a similar working scheme. A pulsed laser beam is focused on the sample. The photoluminescence from the sample is collimated and collected by a photodetector. Transient absorption (TA) is a type of pump-probe spectroscopy that can account for the photo-generated carriers in semiconductors.

Time-Correlated Single Photon Spectroscopy

Time-correlated single photon counting is a statistical method for measuring photoluminescence lifetime with high sensitivity (single-photon level).[127] In this work, a pulsed diode laser, triggered externally at 2.5 MHz, was used to excite the sample at 375 or 438 nm (at a fluence of 1.1×10^{12} photons/cm^2/pulse). The pulse duration of the laser was about 40 ps. The scattered laser light was blocked by different wavelength pass filters and the emitted photons were focused onto a fast avalanche photodiode (SPAD, Micro Photon Devices) with response time less than 50 ps. The full width at half maximum (FWHM) of the instrument response function (IRF) is about 350 ps.

Streak Camera

The streak camera experiment setup is described below. The output of a Ti:Sapphire laser (Spectra−Physics, Tsunami) with 100 fs pulse at 770 nm and at a repetition rate of 81 MHz was used. The excitation light with the wavelength of 385 nm was second harmonic generated by frequency doubling in a beta-barium borate (BBO) crystal and then focused on the samples at an angle of 70°. By a pair of 1 in. quartz plano−convex lenses of 50 mm focal length, the photoluminescence was collected nearly perpendicular to the cuvette plane and focused on the input slit of a spectrograph (Chromex) with 50 lines/mm grating, blazed at 600 nm (2.07 eV). The output of the spectrograph was imaged onto the input slit of the streak camera (Hamamatsu C6860) set at 20 μm. After background subtraction, shading and spectral sensitivity corrections of the measured photoluminescence images were performed with the help of a calibrated reference light source (Ocean Optics, LS−1−CAL).

Transient Absorption

Femtosecond transient absorption spectroscopy (TA) is an extension of steady-state absorption spectroscopy with ultrafast (sub-ps) time resolution. In TA, the samples are initially excited by one laser pulse (the pump beam), then the absorbance of another laser pulse (the probe beam) is detected by the detection system. The TA spectra can be obtained by subtracting the absorbance of the probe beam with and without the pump beam which can be done by blocking the pump with a chopper. The transient absorption spectra with time and energy resolution can be obtained by repeating this at different delay times between the pump and the probe pulse. In the work described in this thesis, TA experiments were performed using a femtosecond pump−probe setup in nitrogen atmosphere. Laser pulses (800 nm, 80 fs pulse length, 1 kHz repetition rate) were generated by a regenerative amplifier (Spitfire XP Pro) seeded by a femtosecond oscillator (Mai Tai SP, both Spectra Physics). The pump pulses at 400 nm were generated by a BBO crystal as a second harmonic of the laser. The used excitation photon fluxes were 1×10^{12} photons/cm^2/pulse. For the probe, the super−continuum generation from a thin CaF_2 plate was used. The mutual polarization between pump and probe beams was set to the magic angle (54.7°) by placing a Berek compensator in the pump beam. The probe pulse and the reference pulse were dispersed in a spectrograph and detected by a diode array (Pascher Instruments). In order to avoid photo−damage, the sample was moved to a fresh spot after each time delay point.

References

1. Vinoth Kanna, I.; Vasudevan, A.; Subramani, K., Internal combustion engine efficiency enhancer by using hydrogen. *Int. J. Ambient Energy* **2020**, *41*, 237-240.
2. Lewis, N. S.; Nocera, D. G., Powering the planet: Chemical challenges in solar energy utilization. *Proc. Natl. Acad. Sci. (USA)* **2006**, *103*, 15729-15735.
3. Council, N. R., The hydrogen economy: opportunities, costs, barriers, and R&D needs. *National Academies Press*, **2004**.
4. Xu, Y.; Zhang, B., Hydrogen photogeneration from water on the biomimetic hybrid artificial photocatalytic systems of semiconductors and earth-abundant metal complexes: progress and challenges. *Catal. Sci. Technol.* **2015**, *5*, 3084-3096.
5. Fujishima, A.; Honda, K., Electrochemical photolysis of water at a semiconductor electrode. *Nature* **1972**, *238*, 37-38.
6. Natali, M., Elucidating the key role of PH on light-driven hydrogen evolution by a molecular cobalt catalyst. *ACS Catal.* **2017**, *7*, 1330-1339.
7. Bamwenda, G. R.; Tsubota, S.; Nakamura, T.; Haruta, M., Photoassisted hydrogen production from a water-ethanol solution: a comparison of activities of Au/TiO_2 and Pt/TiO_2. *J. Photochem. Photobiol. A* **1995**, *89*, 177-189.
8. Berardi, S.; Drouet, S.; Francàs, L.; Gimbert-Suriñach, C.; Guttentag, M.; Richmond, C.; Stoll, T.; Llobet, A., Molecular artificial photosynthesis. *Chem. Soc. Rev.* **2014**, *43*, 7501-7519.
9. Chen, X.; Shen, S.; Guo, L.; Mao, S. S., Semiconductor-based photocatalytic hydrogen generation. *Chem. Rev.* **2010**, *110*, 6503-6570.
10. Hisatomi, T.; Kubota, J.; Domen, K., Recent advances in semiconductors for photocatalytic and photoelectrochemical water splitting. *Chem. Soc. Rev.* **2014**, *43*, 7520-7535.
11. Moniz, S. J.; Shevlin, S. A.; Martin, D. J.; Guo, Z.-X.; Tang, J., Visible-light driven heterojunction photocatalysts for water splitting–a critical review. *Energy Environ. Sci.* **2015**, *8*, 731-759.
12. Zheng, K.; Žídek, K.; Abdellah, M.; Zhang, W.; Chábera, P.; Lenngren, N.; Yartsev, A.; Pullerits, T., Ultrafast charge transfer from CdSe quantum dots to p-type NiO: hole injection vs hole trapping. *J. Phys. Chem. C* **2014**, *118*, 18462-18471.
13. Wen, J.; Xie, J.; Chen, X.; Li, X., A review on g-C_3N_4-based photocatalysts. *Appl. Surf. Sci.* **2017**, *391*, 72-123.

14. Merki, D.; Hu, X., Recent developments of molybdenum and tungsten sulfides as hydrogen evolution catalysts. *Energy Environ. Sci.* **2011**, *4*, 3878-3888.
15. Frey, M., Hydrogenases: hydrogen‐activating enzymes. *ChemBioChem* **2002**, *3*, 153-160.
16. Tard, C.; Pickett, C. J., Structural and functional analogues of the active sites of the [Fe]-,[NiFe]-, and [FeFe]-hydrogenases. *Chem. Rev.* **2009**, *109*, 2245-2274.
17. Rodenberg, A.; Orazietti, M.; Probst, B.; Bachmann, C.; Alberto, R.; Baldridge, K. K.; Hamm, P., Mechanism of photocatalytic hydrogen generation by a polypyridyl-based cobalt catalyst in aqueous solution. *Inorg. Chem.* **2015**, *54*, 646-657.
18. Chen, F.; Huang, H.; Guo, L.; Zhang, Y.; Ma, T., The role of polarization in photocatalysis. *Angew. Chem. Int. Ed.* **2019**, *58*, 10061-10073.
19. Li, X.-B.; Tung, C.-H.; Wu, L.-Z., Semiconducting quantum dots for artificial photosynthesis. *Nat. Rev. Chem.* **2018**, *2*, 160-173.
20. Nalwa, H. S., Handbook of nanostructured materials and nanotechnology, five-volume set. *Academic Press*, **1999**.
21. Smith, A. M.; Nie, S., Semiconductor nanocrystals: structure, properties, and band gap engineering. *Acc. Chem. Res.* **2010**, *43*, 190-200.
22. Rogach, A. L.; Kornowski, A.; Gao, M.; Eychmüller, A.; Weller, H., Synthesis and characterization of a size series of extremely small thiol-stabilized CdSe nanocrystals. *J. Phys. Chem. B* **1999**, *103*, 3065-3069.
23. Aldana, J.; Wang, Y. A.; Peng, X., Photochemical instability of CdSe nanocrystals coated by hydrophilic thiols. *J. Am. Chem. Soc.* **2001**, *123*, 8844-8850.
24. Aldana, J.; Lavelle, N.; Wang, Y.; Peng, X., Size-dependent dissociation pH of thiolate ligands from cadmium chalcogenide nanocrystals. *J. Am. Chem. Soc.* **2005**, *127*, 2496-2504.
25. Li, C.; Rahaman, A.; Lin, W.; Mourad, H.; Meng, J.; Honarfar, A.; Abdellah, M.; Guo, M.; Richmond, M. G.; Nordlander, E., Electron transfer mediated by iron carbonyl clusters enhance light‐driven hydrogen evolution in water by quantum dots. *ChemSusChem* **2020**, *13*, 3252-3260.
26. Wang, X.; Maeda, K.; Thomas, A.; Takanabe, K.; Xin, G.; Carlsson, J. M.; Domen, K.; Antonietti, M., A metal-free polymeric photocatalyst for hydrogen production from water under visible light. *Nat. Mater.* **2009**, *8*, 76-80.
27. Cao, S.; Low, J.; Yu, J.; Jaroniec, M., Polymeric photocatalysts based on graphitic carbon nitride. *Adv. Mater.* **2015**, *27*, 2150-2176.
28. Zheng, Y.; Liu, J.; Liang, J.; Jaroniec, M.; Qiao, S. Z., Graphitic carbon nitride materials: controllable synthesis and applications in fuel cells and photocatalysis. *Energy Environ. Sci.* **2012**, *5*, 6717-6731.
29. Stoll, T.; Castillo, C. E.; Kayanuma, M.; Sandroni, M.; Daniel, C.; Odobel, F.; Fortage, J.; Collomb, M.-N., Photo-induced redox catalysis for proton

reduction to hydrogen with homogeneous molecular systems using rhodium-based catalysts. *Coord. Chem. Rev.* **2015**, *304*, 20-37.
30. Lehn, J. M., Chemical storage of light energy catalytic generation of hydrogen by visible light or sunlight irradiation of neutral aqueous solutions. *Nouv. J. Chim.* **1977**, *1*, 449-451.
31. Moradpour, A., Hydrogen production by visible light irradiation of aqueous solutions of Ru $(bpy)_3^{2+}$. *Nouv. J. Chim.* **1978**, *2*, 547-549.
32. Kalyanasundaram, K.; Kiwi, J.; Grätzel, M., Hydrogen evolution from water by visible light, a homogeneous three component test system for redox catalysis. *Helv. Chim. Acta* **1978**, *61*, 2720-2730.
33. Wang, Q.; Domen, K., Particulate photocatalysts for light-driven water splitting: mechanisms, challenges, and design strategies. *Chem. Rev.* **2019**, *120*, 919-985.
34. Dalle, K. E.; Warnan, J.; Leung, J. J.; Reuillard, B.; Karmel, I. S.; Reisner, E., Electro-and solar-driven fuel synthesis with first row transition metal complexes. *Chem. Rev.* **2019**, *119*, 2752-2875.
35. Wang, M.; Han, K.; Zhang, S.; Sun, L., Integration of organometallic complexes with semiconductors and other nanomaterials for photocatalytic H_2 production. *Coord. Chem. Rev.* **2015**, *287*, 1-14.
36. Cammack, R., Hydrogenase sophistication. *Nature* **1999**, *397*, 214-215.
37. Wu, L.-Z.; Chen, B.; Li, Z.-J.; Tung, C.-H., Enhancement of the efficiency of photocatalytic reduction of protons to hydrogen via molecular assembly. *Acc. Chem. Res.* **2014**, *47*, 2177-2185.
38. Wang, F.; Wang, W. G.; Wang, X. J.; Wang, H. Y.; Tung, C. H.; Wu, L. Z., A highly efficient photocatalytic system for hydrogen production by a robust hydrogenase mimic in an aqueous solution. *Angew. Chem. Int. Ed.* **2011**, *50*, 3193-3197.
39. Jian, J.-X.; Liu, Q.; Li, Z.-J.; Wang, F.; Li, X.-B.; Li, C.-B.; Liu, B.; Meng, Q.-Y.; Chen, B.; Feng, K., Chitosan confinement enhances hydrogen photogeneration from a mimic of the diiron subsite of [FeFe]-hydrogenase. *Nat. Commun.* **2013**, *4*, 1-9.
40. Li, C.-B.; Li, Z.-J.; Yu, S.; Wang, G.-X.; Wang, F.; Meng, Q.-Y.; Chen, B.; Feng, K.; Tung, C.-H.; Wu, L.-Z., Interface-directed assembly of a simple precursor of [FeFe]–H_2ase mimics on CdSe QDs for photosynthetic hydrogen evolution in water. *Energy Environ. Sci.* **2013**, *6*, 2597-2602.
41. Song, X. W.; Wen, H. M.; Ma, C. B.; Hu, M. Q.; Chen, H.; Cui, H. H.; Chen, C. N., Photocatalytic hydrogen evolution by two comparable [FeFe] ‐ hydrogenase mimics assembled to the surface of ZnS. *Appl. Organomet. Chem.* **2014**, *28*, 267-273.
42. Rahaman, A., Lisensky, G.C., Browder-Long, J., Hrovat, D.A., Richmond, M.G., Nordlander, E. and Hogarth, G., Electrocatalytic proton-reduction behaviour of telluride-capped triiron clusters: tuning of overpotentials and stabilization of redox states relative to lighter chalcogenide analogues. *Dalton Trans.*, **2020**, *49*, 7133-7143.

43. Lesch, D. A.; Rauchfuss, T. B., Isolation and characterization of $Fe_2(\mu\text{-}Te_2)(CO)_6$ and its conversion to $Fe_3(\mu_3\text{-}Te)_2(CO)_x$ (x= 9, 10). *Inorg. Chem.* **1981**, *20*, 3583-3585.
44. Han, Z.; Qiu, F.; Eisenberg, R.; Holland, P. L.; Krauss, T. D., Robust photogeneration of H_2 in water using semiconductor nanocrystals and a nickel catalyst. *Science* **2012**, *338*, 1321-1324.
45. Liu, C.; Qiu, F.; Peterson, J. J.; Krauss, T. D., Aqueous photogeneration of H_2 with CdSe nanocrystals and nickel catalysts: electron transfer dynamics. *J. Phys. Chem. B* **2015**, *119*, 7349-7357.
46. Wen, F.; Yang, J.; Zong, X.; Ma, B.; Wang, D.; Li, C., Photocatalytic H_2 production on hybrid catalyst system composed of inorganic semiconductor and cobaloximes catalysts. *J. Catal.* **2011**, *281*, 318-324.
47. Huang, J.; Mulfort, K. L.; Du, P.; Chen, L. X., Photodriven charge separation dynamics in CdSe/ZnS core/shell quantum dot/cobaloxime hybrid for efficient hydrogen production. *J. Am. Chem. Soc.* **2012**, *134*, 16472-16475.
48. Gimbert-Suriñach, C.; Albero, J.; Stoll, T.; Fortage, J.; Collomb, M.-N.; Deronzier, A.; Palomares, E.; Llobet, A., Efficient and limiting reactions in aqueous light-induced hydrogen evolution systems using molecular catalysts and quantum dots. *J. Am. Chem. Soc.* **2014**, *136*, 7655-7661.
49. Wang, X.; Li, C., Interfacial charge transfer in semiconductor-molecular photocatalyst systems for proton reduction. *J. Photochem. Photobiol. C* **2017**, *33*, 165-179.
50. Harris, R. D.; Bettis Homan, S.; Kodaimati, M.; He, C.; Nepomnyashchii, A. B.; Swenson, N. K.; Lian, S.; Calzada, R.; Weiss, E. A., Electronic processes within quantum dot-molecule complexes. *Chem. Rev.* **2016**, *116*, 12865-12919.
51. Schnitzenbaumer, K. J.; Labrador, T.; Dukovic, G., Impact of chalcogenide ligands on excited state dynamics in CdSe quantum dots. *J. Phys. Chem. C* **2015**, *119*, 13314-13324.
52. Ong, W.-J.; Tan, L.-L.; Ng, Y. H.; Yong, S.-T.; Chai, S.-P., Graphitic carbon nitride (g-C3N4)-based photocatalysts for artificial photosynthesis and environmental remediation: are we a step closer to achieving sustainability? *Chem. Rev.* **2016**, *116*, 7159-7329.
53. Ren, Y.; Zeng, D.; Ong, W.-J., Interfacial engineering of graphitic carbon nitride (g-C3N4)-based metal sulfide heterojunction photocatalysts for energy conversion: a review. *Chinese J. Catal.* **2019**, *40*, 289-319.
54. Fu, J.; Chang, B.; Tian, Y.; Xi, F.; Dong, X., Novel C_3N_4–CdS composite photocatalysts with organic–inorganic heterojunctions: in situ synthesis, exceptional activity, high stability and photocatalytic mechanism. *J. Mater. Chem. A* **2013**, *1*, 3083-3090.
55. Zhong, Y.; Chen, W.; Yu, S.; Xie, Z.; Wei, S.; Zhou, Y., CdSe quantum dots/g-C_3N_4 heterostructure for efficient H_2 production under visible light irradiation. *ACS Omega* **2018**, *3*, 17762-17769.
56. Zhou, P.; Yu, J.; Jaroniec, M., All‐solid‐state Z‐scheme photocatalytic systems. *Adv. Mater.* **2014**, *26*, 4920-4935.

57. Vattikuti, S. P.; Reddy, P. A. K.; Shim, J.; Byon, C., Visible-Light-Driven Photocatalytic Activity of SnO_2–ZnO Quantum Dots Anchored on g-C_3N_4 Nanosheets for Photocatalytic Pollutant Degradation and H_2 Production. *ACS Omega* **2018**, *3*, 7587-7602.
58. Marchal, C.; Cottineau, T.; Méndez‐Medrano, M. G.; Colbeau‐Justin, C.; Caps, V.; Keller, V., Au/TiO_2 ‐ g-C_3N_4 nanocomposites for enhanced photocatalytic H_2 production from water under visible light irradiation with very low quantities of sacrificial agents. *Adv. Energy Mater.* **2018**, *8*, 1702142.
59. Zidek, K.; Zheng, K.; Ponseca Jr, C. S.; Messing, M. E.; Wallenberg, L. R.; Chábera, P.; Abdellah, M.; Sundström, V.; Pullerits, T., Electron transfer in quantum-dot-sensitized ZnO nanowires: ultrafast time-resolved absorption and terahertz study. *J. Am. Chem. Soc.* **2012**, *134*, 12110-12117.
60. Li, C.; Zou, X.; Lin, W.; Mourad, H.; Meng, J.; Liu, Y.; Abdellah, M.; Guo, M.; Zheng, K.; Nordlander, E., A graphitic carbon nitride/CdSe quantum dot/iron carbonyl cluster composite for enhanced photocatalytic hydrogen evolution. *manuscript*.
61. Call, A.; Codolà, Z.; Acuña‐Parés, F.; Lloret‐Fillol, J., Photo‐and electrocatalytic H_2 production by new first‐row transition‐metal complexes based on an aminopyridine pentadentate ligand. *Chem. Eur. J.* **2014**, *20*, 6171-6183.
62. Kanan, M. W.; Nocera, D. G., In situ formation of an oxygen-evolving catalyst in neutral water containing phosphate and Co^{2+}. *Science* **2008**, *321*, 1072-1075.
63. Surendranath, Y.; Dinca, M.; Nocera, D. G., Electrolyte-dependent electrosynthesis and activity of cobalt-based water oxidation catalysts. *J. Am. Chem. Soc.* **2009**, *131*, 2615-2620.
64. Risch, M.; Khare, V.; Zaharieva, I.; Gerencser, L.; Chernev, P.; Dau, H., Cobalt− oxo core of a water-oxidizing catalyst film. *J. Am. Chem. Soc.* **2009**, *131*, 6936-6937.
65. Kanan, M. W.; Yano, J.; Surendranath, Y.; Dinca, M.; Yachandra, V. K.; Nocera, D. G., Structure and valency of a cobalt− phosphate water oxidation catalyst determined by in situ X-ray spectroscopy. *J. Am. Chem. Soc.* **2010**, *132*, 13692-13701.
66. McAlpin, J. G.; Stich, T. A.; Ohlin, C. A.; Surendranath, Y.; Nocera, D. G.; Casey, W. H.; Britt, R. D., Electronic structure description of a $[Co(III)_3Co(IV)O_4]$ cluster: a model for the paramagnetic intermediate in cobalt-catalyzed water oxidation. *J. Am. Chem. Soc.* **2011**, *133*, 15444-15452.
67. Wasylenko, D. J.; Palmer, R. D.; Berlinguette, C. P., Homogeneous water oxidation catalysts containing a single metal site. *Chem. Commun.* **2013**, *49*, 218-227.
68. Wasylenko, D. J.; Ganesamoorthy, C.; Borau-Garcia, J.; Berlinguette, C. P., Electrochemical evidence for catalyticwater oxidation mediated by a high-valent cobalt complex. *Chem. Commun.* **2011**, *47*, 4249-4251.

69. Zhao, X.; Wang, P.; Long, M., Electro-and photocatalytic hydrogen production by molecular cobalt complexes with pentadentate ligands. *Comments Inorg. Chem.* **2017**, *37*, 238-270.
70. Wang, P.; Liang, G.; Reddy, M. R.; Long, M.; Driskill, K.; Lyons, C.; Donnadieu, B.; Bollinger, J. C.; Webster, C. E.; Zhao, X., Electronic and steric tuning of catalytic H_2 evolution by cobalt complexes with pentadentate polypyridyl-amine ligands. *J. Am. Chem. Soc.* **2018**, *140*, 9219-9229.
71. Sun, Y.; Bigi, J. P.; Piro, N. A.; Tang, M. L.; Long, J. R.; Chang, C. J., Molecular cobalt pentapyridine catalysts for generating hydrogen from water. *J. Am. Chem. Soc.* **2011**, *133*, 9212-9215.
72. Sun, Y.; Sun, J.; Long, J. R.; Yang, P.; Chang, C. J., Photocatalytic generation of hydrogen from water using a cobalt pentapyridine complex in combination with molecular and semiconductor nanowire photosensitizers. *Chem. Sci.* **2013**, *4*, 118-124.
73. Nippe, M.; Khnayzer, R. S.; Panetier, J. A.; Zee, D. Z.; Olaiya, B. S.; Head-Gordon, M.; Chang, C. J.; Castellano, F. N.; Long, J. R., Catalytic proton reduction with transition metal complexes of the redox-active ligand bpy_2PYMe. *Chem. Sci.* **2013**, *4*, 3934-3945.
74. Jurss, J. W.; Khnayzer, R. S.; Panetier, J. A.; El Roz, K. A.; Nichols, E. M.; Head-Gordon, M.; Long, J. R.; Castellano, F. N.; Chang, C. J., Bioinspired design of redox-active ligands for multielectron catalysis: effects of positioning pyrazine reservoirs on cobalt for electro-and photocatalytic generation of hydrogen from water. *Chem. Sci.* **2015**, *6*, 4954-4972.
75. Chen, L.; Khadivi, A.; Singh, M.; Jurss, J. W., Synthesis of a pentadentate, polypyrazine ligand and its application in cobalt-catalyzed hydrogen production. *Inorg. Chem. Front.* **2017**, *4*, 1649-1653.
76. Bachmann, C.; Guttentag, M.; Spingler, B.; Alberto, R., 3d Element complexes of pentadentate bipyridine-pyridine-based ligand scaffolds: structures and photocatalytic activities. *Inorg. Chem.* **2013**, *52*, 6055-6061.
77. Deponti, E.; Luisa, A.; Natali, M.; Iengo, E.; Scandola, F., Photoinduced hydrogen evolution by a pentapyridine cobalt complex: elucidating some mechanistic aspects. *Dalton Trans.* **2014**, *43*, 16345-16353.
78. Singh, W. M.; Baine, T.; Kudo, S.; Tian, S.; Ma, X. A. N.; Zhou, H.; DeYonker, N. J.; Pham, T. C.; Bollinger, J. C.; Baker, D. L., Electrocatalytic and photocatalytic hydrogen production in aqueous solution by a molecular cobalt complex. *Angew. Chem. Int. Ed.* **2012**, *51*, 5941-5944.
79. Shan, B.; Baine, T.; Ma, X. A. N.; Zhao, X.; Schmehl, R. H., Mechanistic details for cobalt catalyzed photochemical hydrogen production in aqueous solution: Efficiencies of the photochemical and non-photochemical steps. *Inorg. Chem.* **2013**, *52*, 4853-4859.
80. Vennampalli, M.; Liang, G.; Katta, L.; Webster, C. E.; Zhao, X., Electronic effects on a mononuclear Co complex with a pentadentate ligand for catalytic H_2 evolution. *Inorg. Chem.* **2014**, *53*, 10094-10100.
81. Xie, J.; Zhou, Q.; Li, C.; Wang, W.; Hou, Y.; Zhang, B.; Wang, X., An unexpected role of the monodentate ligand in photocatalytic hydrogen

production of the pentadentate ligand-based cobalt complexes. *Chem. Commun.* **2014**, *50*, 6520-6522.
82. Lo, W. K.; Castillo, C. E.; Gueret, R.; Fortage, J. r. m.; Rebarz, M.; Sliwa, M.; Thomas, F.; McAdam, C. J.; Jameson, G. B.; McMorran, D. A., Synthesis, characterization, and photocatalytic H2-evolving activity of a family of [Co(N4Py)(X)]n+ complexes in aqueous solution. Inorg. Chem. 2016, 55, 4564-4581.
83. Zhang, P.; Wang, M.; Gloaguen, F.; Chen, L.; Quentel, F.; Sun, L., Electrocatalytic hydrogen evolution from neutral water by molecular cobalt tripyridine–diamine complexes. *Chem. Commun.* **2013**, *49*, 9455-9457.
84. Basu, D.; Mazumder, S.; Shi, X.; Baydoun, H.; Niklas, J.; Poluektov, O.; Schlegel, H. B.; Verani, C. N., Ligand transformations and efficient proton/water reduction with cobalt catalysts based on pentadentate pyridine‐rich environments. *Angew. Chem. Int. Ed.* **2015**, *54*, 2105-2110.
85. Li, C.; Li, Y.; Li, Y.; Hossain, M. K.; Guo, M.; Haukka, M.; Dietzek, B.; Nordlander, E., Photoinduced hydrogen evolution catalyzed by new Co(II) complexes of N5-donor ligands. *manuscript.*
86. Lewandowska-Andralojc, A.; Baine, T.; Zhao, X.; Muckerman, J. T.; Fujita, E.; Polyansky, D. E., Mechanistic studies of hydrogen evolution in aqueous solution catalyzed by a terpyridine–amine cobalt complex. *Inorg. Chem.* **2015**, *54*, 4310-4321.
87. Kayanuma, M.; Stoll, T.; Daniel, C.; Odobel, F.; Fortage, J.; Deronzier, A.; Collomb, M.-N., A computational mechanistic investigation of hydrogen production in water using the $[RhIII(dmbpy)_2Cl_2]^+$/$[RuII(bpy)_3]^{2+}$/ascorbic acid photocatalytic system. *Phys. Chem. Chem. Phys.* **2015**, *17*, 10497-10509.
88. Solis, B. H.; Hammes-Schiffer, S., Theoretical analysis of mechanistic pathways for hydrogen evolution catalyzed by cobaloximes. *Inorg. Chem.* **2011,** *50*, 11252-11262.
89. Solis, B. H.; Hammes-Schiffer, S., Substituent effects on cobalt diglyoxime catalysts for hydrogen evolution. *J. Am. Chem. Soc.* **2011**, *133*, 19036-19039.
90. Muckerman, J. T.; Fujita, E., Theoretical studies of the mechanism of catalytic hydrogen production by a cobaloxime. *Chem. Commun.* **2011**, *47*, 12456-12458.
91. Bhattacharjee, A.; Chavarot-Kerlidou, M.; Andreiadis, E. S.; Fontecave, M.; Field, M. J.; Artero, V., Combined experimental–theoretical characterization of the hydrido-cobaloxime $[HCo(dmgH)_2(P_nBu_3)]$. *Inorg. Chem.* **2012**, *51*, 7087-7093.
92. Jiang, Y. K.; Liu, J. H., DFT studies of cobalt hydride intermediate on cobaloxime‐catalyzed H_2 evolution pathways. *Int. J. Quantum Chem.* **2012**, *112*, 2541-2546.
93. Bhattacharjee, A.; Andreiadis, E. S.; Chavarot‐Kerlidou, M.; Fontecave, M.; Field, M. J.; Artero, V., A computational study of the mechanism of hydrogen evolution by cobalt (diimine‐dioxime) catalysts. *Chem. Eur. J.* **2013**, *19*, 15166-15174.

94. Solis, B. H.; Yu, Y.; Hammes-Schiffer, S., Effects of ligand modification and protonation on metal oxime hydrogen evolution electrocatalysts. *Inorg. Chem.* **2013**, *52*, 6994-6999.
95. Wang, P.; Liang, G.; Smith, N.; Hill, K.; Donnadieu, B.; Webster, C. E.; Zhao, X., Enhanced hydrogen evolution in neutral water catalyzed by a cobalt complex with a softer polypyridyl ligand. *Angew. Chem. Int. Ed.* **2020**, *132*, 12794-12797.
96. Guo, Y.; Park, T.; Yi, J. W.; Henzie, J.; Kim, J.; Wang, Z.; Jiang, B.; Bando, Y.; Sugahara, Y.; Tang, J., Nanoarchitectonics for transition‐metal‐sulfide‐based electrocatalysts for water splitting. *Adv. Mater.* **2019**, *31*, 1807134.
97. Yan, Y.; He, T.; Zhao, B.; Qi, K.; Liu, H.; Xia, B. Y., Metal/covalent–organic frameworks-based electrocatalysts for water splitting. *J. Mater. Chem. A* **2018**, *6*, 15905-15926.
98. Yu, M.; Zhao, S.; Feng, H.; Hu, L.; Zhang, X.; Zeng, Y.; Tong, Y.; Lu, X., Engineering thin MoS_2 nanosheets on TiN nanorods: advanced electrochemical capacitor electrode and hydrogen evolution electrocatalyst. *ACS Energy Lett.* **2017**, *2*, 1862-1868.
99. Sun, Y.; Alimohammadi, F.; Zhang, D.; Guo, G., Enabling colloidal synthesis of edge-oriented MoS2 with expanded interlayer spacing for enhanced HER catalysis. *Nano Lett.* **2017**, *17*, 1963-1969.
100. Jaramillo, T. F.; Jørgensen, K. P.; Bonde, J.; Nielsen, J. H.; Horch, S.; Chorkendorff, I., Identification of active edge sites for electrochemical H_2 evolution from MoS_2 nanocatalysts. *Science* **2007**, *317*, 100-102.
101. Wang, F.; Shifa, T. A.; Zhan, X.; Huang, Y.; Liu, K.; Cheng, Z.; Jiang, C.; He, J., Recent advances in transition-metal dichalcogenide based nanomaterials for water splitting. *Nanoscale* **2015**, *7*, 19764-19788.
102. Yan, Y.; Xia, B.; Xu, Z.; Wang, X., Recent development of molybdenum sulfides as advanced electrocatalysts for hydrogen evolution reaction. *ACS Catal.* **2014**, *4*, 1693-1705.
103. Geng, X.; Sun, W.; Wu, W.; Chen, B.; Al-Hilo, A.; Benamara, M.; Zhu, H.; Watanabe, F.; Cui, J.; Chen, T.-P., Pure and stable metallic phase molybdenum disulfide nanosheets for hydrogen evolution reaction. *Nat. Commun.* **2016**, *7*, 1-7.
104. Tan, C.; Luo, Z.; Chaturvedi, A.; Cai, Y.; Du, Y.; Gong, Y.; Huang, Y.; Lai, Z.; Zhang, X.; Zheng, L., Preparation of high‐percentage 1T‐phase transition metal dichalcogenide nanodots for electrochemical hydrogen evolution. *Adv. Mater.* **2018**, *30*, 1705509.
105. Heydari-Bafrooei, E.; Askari, S., Electrocatalytic activity of MWCNT supported Pd nanoparticles and MoS_2 nanoflowers for hydrogen evolution from acidic media. *Int. J. Hydrogen Energy* **2017**, *42*, 2961-2969.
106. Gopalakrishnan, D.; Damien, D.; Shaijumon, M. M., MoS_2 quantum dot-interspersed exfoliated MoS_2 nanosheets. *ACS Nano* **2014**, *8*, 5297-5303.
107. Xi, F.; Bogdanoff, P.; Harbauer, K.; Plate, P.; Höhn, C.; Rappich, J. r.; Wang, B.; Han, X.; van de Krol, R.; Fiechter, S., Structural transformation identification of sputtered amorphous MoS_x as an efficient hydrogen-

evolving catalyst during electrochemical activation. *ACS Catal.* **2019**, *9*, 2368-2380.
108. Li, L.; Qin, Z.; Ries, L.; Hong, S.; Michel, T.; Yang, J.; Salameh, C.; Bechelany, M.; Miele, P.; Kaplan, D., Role of sulfur vacancies and undercoordinated Mo regions in MoS_2 nanosheets toward the evolution of hydrogen. *ACS Nano* **2019**, *13*, 6824-6834.
109. Li, H.; Tsai, C.; Koh, A. L.; Cai, L.; Contryman, A. W.; Fragapane, A. H.; Zhao, J.; Han, H. S.; Manoharan, H. C.; Abild-Pedersen, F., Activating and optimizing MoS_2 basal planes for hydrogen evolution through the formation of strained sulphur vacancies. *Nat. Mater.* **2016**, *15*, 48-53.
110. Tran, P. D.; Tran, T. V.; Orio, M.; Torelli, S.; Truong, Q. D.; Nayuki, K.; Sasaki, Y.; Chiam, S. Y.; Yi, R.; Honma, I., Coordination polymer structure and revisited hydrogen evolution catalytic mechanism for amorphous molybdenum sulfide. *Nat. Mater.* **2016**, *15*, 640-646.
111. Li, Y.; Wang, H.; Xie, L.; Liang, Y.; Hong, G.; Dai, H., MoS2 nanoparticles grown on graphene: an advanced catalyst for the hydrogen evolution reaction. *J. Am. Chem. Soc.* **2011**, *133*, 7296-7299.
112. Huang, Z.; Luo, W.; Ma, L.; Yu, M.; Ren, X.; He, M.; Polen, S.; Click, K.; Garrett, B.; Lu, J., Dimeric $[Mo_2S_{12}]^{2-}$ cluster: a molecular analogue of MoS_2 edges for superior hydrogen‐evolution electrocatalysis. *Angew. Chem. Int. Ed.* **2015**, *54*, 15181-15185.
113. Merki, D.; Fierro, S.; Vrubel, H.; Hu, X., Amorphous molybdenum sulfide films as catalysts for electrochemical hydrogen production in water. *Chem. Sci.* **2011**, *2*, 1262-1267.
114. Chang, Y. H.; Lin, C. T.; Chen, T. Y.; Hsu, C. L.; Lee, Y. H.; Zhang, W.; Wei, K. H.; Li, L. J., Highly efficient electrocatalytic hydrogen production by MoSx grown on graphene‐protected 3D Ni foams. *Adv. Mater.* **2013**, *25*, 756-760.
115. Grutza, M.-L.; Rajagopal, A.; Streb, C.; Kurz, P., Hydrogen evolution catalysis by molybdenum sulfides (MoS x): are thiomolybdate clusters like $[Mo_3S_{13}]^{2-}$ suitable active site models? *Sustain. Energy Fuels* **2018**, *2*, 1893-1904.
116. Kibsgaard, J.; Jaramillo, T. F.; Besenbacher, F., Building an appropriate active-site motif into a hydrogen-evolution catalyst with thiomolybdate $[Mo_3S_{13}]^{2-}$ clusters. *Nat. Chem.* **2014**, *6*, 248.
117. Jaramillo, T. F.; Bonde, J.; Zhang, J.; Ooi, B.-L.; Andersson, K.; Ulstrup, J.; Chorkendorff, I., Hydrogen evolution on supported incomplete cubane-type $[Mo_3S_4]^{4+}$ electrocatalysts. *J. Phys. Chem. C* **2008**, *112*, 17492-17498.
118. Karunadasa, H. I.; Montalvo, E.; Sun, Y.; Majda, M.; Long, J. R.; Chang, C. J., A molecular MoS_2 edge site mimic for catalytic hydrogen generation. *Science* **2012**, *335*, 698-702.
119. Ji, Z.; Trickett, C.; Pei, X.; Yaghi, O. M., Linking molybdenum–sulfur clusters for electrocatalytic hydrogen evolution. *J. Am. Chem. Soc.* **2018**, *140*, 13618-13622.

120. Dave, M.; Rajagopal, A.; Damm-Ruttensperger, M.; Schwarz, B.; Nägele, F.; Daccache, L.; Fantauzzi, D.; Jacob, T.; Streb, C., Understanding homogeneous hydrogen evolution reactivity and deactivation pathways of molecular molybdenum sulfide catalysts. *Sustain. Energy Fuels* **2018**, *2*, 1020-1026.
121. Lei, Y.; Yang, M.; Hou, J.; Wang, F.; Cui, E.; Kong, C.; Min, S., Thiomolybdate $[Mo^3S_{13}]^{2-}$ nanocluster: a molecular mimic of MoS_2 active sites for highly efficient photocatalytic hydrogen evolution. *Chem. Commun.* **2018,** *54*, 603-606.
122. Rajagopal, A.; Venter, F.; Jacob, T.; Petermann, L.; Rau, S.; Tschierlei, S.; Streb, C., Homogeneous visible light-driven hydrogen evolution by the molecular molybdenum sulfide model $[Mo_2S_{12}]^{2-}$. *Sustain. Energy Fuels* **2019**, *3*, 92-95.
123. Li, C.; Zou, X.; Mourad, H.; Li Y.; Lin W.; Zheng K.; Nordlander, E., Oligomeric and polymeric molybdenum sulfide cluster catalysts for light−driven hydrogen evolution: catalysis and carrier recombination dynamics. *manuscript*.
124. Artero, V.; Fontecave, M., Solar fuels generation and molecular systems: is it homogeneous or heterogeneous catalysis? *Chem. Soc. Rev.* **2013**, *42*, 2338-2356.
125. Cobo, S.; Heidkamp, J.; Jacques, P.-A.; Fize, J.; Fourmond, V.; Guetaz, L.; Jousselme, B.; Ivanova, V.; Dau, H.; Palacin, S., A Janus cobalt-based catalytic material for electro-splitting of water. *Nat. Mater.* **2012**, *11*, 802-807.
126. Basu, D.; Mazumder, S.; Shi, X.; Staples, R. J.; Schlegel, H. B.; Verani, C. N., Distinct proton and water reduction behavior with a cobalt (III) electrocatalyst based on pentadentate oximes. *Angew. Chem. Int. Ed.* **2015**, *127*, 7245-7249.
127. Becker, W.; Hickl, H.; Zander, C.; Drexhage, K.; Sauer, M.; Siebert, S.; Wolfrum, J., Time-resolved detection and identification of single analyte molecules in microcapillaries by time-correlated single-photon counting (TCSPC). *Rev. Sci. Instrum.* **1999**, *70*, 1835-1841.